

Reply to Referee #1

Ref: Atmos. Chem. Phys. Discuss., acp-2018-1361, Jun 12, 2019

Title: "Winter 2018 major sudden stratospheric warming impact on midlatitude mesosphere from microwave radiometer measurements" by Yuke Wang et al.

We thank Referee #1 once again for very useful comments, discussion and proposals for corrections. We made corrections and changed the text according to the suggestions. Our revisions and reply to the Referee #1 comments are below in blue colored text.

Referee Comment: RC

Authors Comment: AC

RC: GENERAL COMMENTS

The authors have taken my comments and suggestions carefully into account. Further, they added a wavenumber analysis which, however, does not support the aim of the paper. This is in the interpretation of local mesosphere microwave radiometer observations. So, either the wavenumber analysis of satellite observations is taken out or it is related to the MWR time series. A related major revision should include a careful re-edition.

RC: SPECIFIC COMMENTS

There are two options which have to be decided upon: either concentration of the paper (1) or extension (2). In any case, a homogenization (3) is due.

1) Concentration: The authors added with sections 4.4 and 5.3 with figures 7, 8, and 9 a wave analysis of MLS temperatures. This analysis does not help the interpretation of the MWR observations, nor does it forward the knowledge on SSWs. Thats why one option is to erase these additions in order to concentrate the paper.

AC: We agree and accept the option (1) proposed by Referee #1 - Concentration - and we corrected the text according this option.

2) Extension: You are presenting wave spectra of MLS temperatures. If it is possible to show a reasonable link to the variability in the MWR carbon monoxide or winds, this would help interpretation of the latter. This could include the fusion of Fig. 8 and 9 for those levels which are shown in Fig. 7. Additionally, a frequency spectrum of MWR wind / carbon monoxide could be shown in another figure. This is the other option.

3) Homogenization: During editing the manuscript, some part of text has doubled and some other technicalities accoured - please, re-edit the text carefully.

AC: We removed and modified the text which was doubled. We re-edited the text as well.

RC: TECHNICAL CORRECTIONS

L296: "descended up to" --> "descended down to" **Corrected, new Line 292.**

L302: "explain causes" --> "suggest causes" because you did not quantitatively separate horizontal and vertical transports nor chemical reactions **Corrected, L298.**

L303: "relative to the pole of the polar vortex" --> "of the polar vortex relative to the pole" [Corrected, L300](#).

L313: "easterly domination" --> "dominance of easterlies" [Corrected, L309](#).

L362: "although" --> "while" [Corrected, L357](#).

L362: In fig. 6a, it is rather the -50-degree-contour than the -55-degree-contour which is descending, or? [Corrected, L387](#).

L395:

"does not accompany by" --> "is not associated with" or "is not accompanied by" [Corrected, L390](#).
"coupling observed" --> "coupling as observed" [Corrected, L390](#).

L422: "transformation" --> "propagation" [Text deleted](#).

L428: End the sentence after "altitude" --> "... altitude. Fig. 8..." [Text deleted](#).

L489: The sentence "The horizontal CO gradient at the polar vortex edge also exists and the vortex split and displacement of the pole associated with the SSW cause significant CO variability at the NH midlatitudes" is highly confusing. Perhaps, it could better express what you mean with "Because of the horizontal CO gradient at the polar vortex edge its split and displacement during the SSW cause a significant CO variability at the NH midlatitudes"? [Corrected, L420-421](#).

L647-L659: This paragraph from "Among the..." to "...split event." is exactly the same as in L470-L481. Please, re-edit this doubling.

AC: The text rephrased and left in Conclusions only.

Fig. 8: The eastward wave 2 should be marked blue in the frequency-wavenumber plot (right column). [Fig. 8 removed from the text](#).

Fig. 9: In the spectra for 20 Dec - 10 Feb (left column) you associated eastward wave 2 with a blue line but do not show it in the spectrum. This wave type is also not indicated in the frequency-wavenumber plots (right column). [Fig. 9 removed from the text](#).

Reply to Referee #2

Ref: Atmos. Chem. Phys. Discuss., acp-2018-1361, Jun 12, 2019

Title: "Winter 2018 major sudden stratospheric warming impact on midlatitude mesosphere from microwave radiometer measurements" by Yuke Wang et al.

We thank Referee #2 once again for useful comments, discussion and proposals for corrections. We have included corrections and changes in the text according suggestions. Our revisions and reply to Referee #2 comments are below in blue colored text. RC (AC) is Referee (Authors) comments. Line numbers of the revised manuscript are indicated.

Referee # 2

Comments on "Winter 2018 major sudden stratospheric warming impact on midlatitude mesosphere from microwave radiometer measurements" by Yuke Wang, Valeri Shulga, Gennadi Milnevsky, et al. (2019).

RC: The general quality of the revised manuscript is greatly improved, compared with the original version. I only have very tiny minor comments this time that should be corrected before publication.

P42: "each two years", better to say "every other year" **Corrected, new Line43.**

P76: "following" or "followed by"? I guess the latter. **Corrected, L80.**

P266: Add "a" before "characteristic". **Corrected, L282.**

P273: What is "the opposite tendency with the stratospheric CO abundance increase"? Why not directly say "A decrease in the stratospheric CO abundance"? **AC:** Corrected to "Unlike the mesosphere, the CO descent and an increase in CO abundance is observed in the stratosphere from both ...", L289.

P276: It is hard for me to understand "descend up". Do you mean "down" rather than "up"? **Corrected, L292.**

P281: What is "by vertical"? A typo? **Corrected, L298-299.**

P283: Better to say "shift between A and B" than "shift in A and B"? **Corrected, L300.**

P293: "Return to" is weird. "Recovery" or "reestablishment" is better. **Corrected, L311.**

P324: "Positive (negative) values are westerly (easterly) wind components." Please delete the non-informative sentence that says nothing. **Deleted**

P335: "Return" is weird. Recovery or reestablishment. **Corrected, L353.**

P337: Move "also" after "is". **Corrected, L355.**

P353: Add a comma after "i.e." **Added, L371.**

P358: "looks about"? Do you mean "The stratosphere is ..."? **Corrected, L377.**

P370: "...does not accompany by" should be "... is not accompanied by" **Corrected, L390.**

P396: Readers will be confused to see "western upper stratosphere".

AC: The text deleted according to proposal of Referee 1 - Concentration.

P414: Count once again to see 40-day or 50-day. **The text deleted.**

P418: "is seen also" should be "is also seen" **The text deleted.**

P419: "If...then..." is an ill sentence. **The text deleted.**

P566: "consistent with" rather "consistent to" **Corrected, L528.**

P619: Change "combine" to "include" **Corrected, L553.**

P630: A typo is here. It should be "higher ...than" rather than "higher ... that". **Corrected, L565.**

New revised texts are below:

1 **Winter 2018 major sudden stratospheric warming impact on midlatitude mesosphere**
2 **from microwave radiometer measurements**

3
4 Yuke Wang¹, Valerii Shulga^{1,2}, Gennadi Milinevsky^{1,3}, Aleksey Patoka², Oleksandr
5 Evtushevsky³, Andrew Klekociuk^{4,5}, Wei Han¹, Asen Grytsai³, Dmitry Shulga², Valery
6 Myshenko², Oleksandr Antyufeyev²

7
8 ¹College of Physics, International Center of Future Science, Jilin University, Changchun,
9 130012, China

10 ²Institute of Radio Astronomy, NAS of Ukraine, Kharkiv, 61002, Ukraine

11 ³Taras Shevchenko National University of Kyiv, Kyiv, 01601, Ukraine

12 ⁴Antarctica and the Global System, Australian Antarctic Division, Kingston, 7050, Australia

13 ⁵Department of Physics, University of Adelaide, Adelaide, 5005, Australia

14

15 *Correspondence to:*

16 Gennadi Milinevsky (genmilinevsky@gmail.com) and Valerii Shulga
17 (shulga@rian.kharkov.ua)

18

19 **Abstract.** The impact of a major sudden stratospheric warming (SSW) in the Arctic in
20 February 2018 on the mid-latitude mesosphere is investigated by performing the microwave
21 radiometer measurements of carbon monoxide (CO) and zonal wind above Kharkiv, Ukraine
22 (50.0°N, 36.3°E). The mesospheric peculiarities of this SSW event were observed using a
23 recently designed and installed microwave radiometer in East Europe for the first time. Data
24 from the ERA-Interim and MERRA-2 reanalyses, as well as the Aura Microwave Limb
25 Sounder measurements, are also used. Microwave observations of the daily CO profiles in
26 January–March 2018 allowed the retrieval of mesospheric zonal wind at 70–85 km (below the
27 winter mesopause) over the Kharkiv site. Reversal of the mesospheric westerly from about 10
28 m s⁻¹ to an easterly wind of about -10 m s⁻¹ around 10 February was observed. The local
29 microwave observations at our NH midlatitude site combined with reanalysis data show wide
30 ranging daily variability in CO, zonal wind and temperature in the mesosphere and stratosphere
31 during the SSW of 2018. The observed local CO variability can be explained mainly by
32 horizontal air mass redistribution due to planetary wave activity. Replacement of the CO-rich
33 polar vortex air by CO-poor air of the surrounding area led to a significant mesospheric CO
34 decrease over the station during the SSW and fragmentation of the vortex over the station at the
35 SSW start caused enhanced stratospheric CO at about 30 km. The results of microwave

36 measurements of CO and zonal wind in the midlatitude mesosphere at 70–85 km altitudes,
37 which still is not adequately covered by ground-based observations, are useful for improving
38 our understanding of the SSW impacts in this region.

39

40

41 **1 Introduction**

42

43 Major sudden stratospheric warming (SSW) events which happen roughly [every other year](#) in
44 the North Polar region are produced by strong planetary wave activity according to the model
45 developed by Matsuno (1971) which is supported by numerous observations (Alexander and
46 Shepherd, 2010; Kuttippurath and Nikulin, 2012; Tao et al., 2015). A major SSW event is
47 accompanied by a sharp increase of the stratosphere temperature up to 50 K and the reversal of
48 the zonal wind from climatological westerlies to easterlies over a period of several days
49 (Charlton and Polvani, 2007; Chandran and Collins, 2014; Hu et al., 2014; Tripathi et al., 2016;
50 Butler et al., 2017; Karpechko et al., 2018; Taguchi, 2018; Rao et al., 2018). The primary
51 definition of a SSW event provided by the World Meteorological Organization requires a
52 stratosphere temperature increase and an accompanying zonal wind reversal to easterlies at the
53 10-hPa pressure level (approximately 30 km altitude) and 60° latitude (WMO, 1978). This
54 definition was broadened and detailed in recent papers (Butler et al., 2015; Butler and Gerber,
55 2018; Rao et al., 2019). The summarizing paper, where a SSW database is described, was
56 published in Butler et al. (2017). This useful tool
57 (<https://www.esrl.noaa.gov/csd/groups/csd8/sswcompendium/>) allows analysis of the
58 conditions in the stratosphere, troposphere, and at the surface before, during and after each
59 SSW event representing its evolution, structure, and impact on winter surface climate. The
60 compendium is based on data from six different reanalysis products, covers the 1958–2014
61 period and includes global daily anomaly fields, full fields, and derived products for each SSW
62 event (Butler et al., 2017).

63 The source of the SSW is planetary wave activity born in the troposphere that propagates
64 upward through the tropopause to the stratosphere (Matsuno, 1971; Alexander and Shepherd,
65 2010, Butler et al., 2015). The enhanced wave activity results in the rapid warming of the polar
66 stratosphere and the breakdown of the stratospheric polar vortex (Matsuno, 1971; de la Torre et
67 al., 2012; Chandran and Collins, 2014; Pedatella et al., 2018). The important feature of a SSW
68 event is its impact on lower altitudes, when temperature and wind anomalies descend
69 downward into the high- and mid-latitude troposphere during the following weeks to month
70 and influence the surface weather (Baldwin and Dunkerton, 2001; Zhou et al., 2002; Butler et

71 al., 2015; Yu et al., 2018). The major SSW events may also impact the atmospheric
72 composition of the whole Northern Hemisphere (NH) stratosphere including mid-latitudes
73 (Solomon et al., 1985; Allen et al., 1999; Tao et al., 2015).

74 During the SSW, vertical coupling covers not only the troposphere but extends upward to
75 the mesosphere. Mesospheric responses to the SSW are observed as enhancement in planetary
76 wave amplitude, zonal wind reversal and significant air cooling (Shepherd et al., 2014; Zülicke
77 and Becker, 2013; Stray et al., 2015; Zülicke et al., 2018), substantial depletion of the metal
78 layers (Feng et al., 2017; Gardner, 2018), mesosphere-to-stratosphere descent of trace species
79 (Manney et al., 2009; Salmi et al., 2011). The SSW events are also accompanied by the rapid
80 descent of the stratopause into the stratosphere at the SSW onset, [followed by](#) formation of the
81 elevated stratopause in the lower mesosphere and gradual stratopause lowering toward its
82 typical position in the SSW recovery phase (Manney et al., 2009; Chandran et al., 2011; Salmi
83 et al., 2011; Tomikawa et al., 2012; Limpasuvan et al., 2016; Orsolini et al., 2010, 2017). The
84 elevated stratopause events provide an evidence of the coupling between the stratosphere and
85 the mesosphere.

86 Among the trace gases, the CO molecule is a good tracer of winter polar vortex dynamics in
87 the upper stratosphere and mesosphere due to its long photochemical lifetime (Solomon et al.,
88 1985; Allen et al., 1999; Rinsland et al., 1999, Shepherd et al. 2014). The CO mixing ratio
89 generally increases with height in the upper stratosphere and mesosphere and increases with
90 latitude toward the winter pole. This is due to the mean meridional circulation which transports
91 CO from the source region in the summer hemisphere and tropics to the extratropical winter
92 mesosphere and stratosphere (Shepherd et al., 2014). Therefore, large abundances of CO appear
93 in the winter polar regions under conditions of large-scale planetary wave activity. Downward
94 meridional transport causes descent of CO between the mesosphere and stratosphere and this
95 process is sensitive to planetary wave amplitudes, and particularly the wave amplitude changes
96 that occur during SSWs (Rinsland et al., 1999; Manney et al., 2009; Kvissel et al., 2012). Due
97 to the large scale descent, high CO values of mesospheric origin are observed at stratospheric
98 altitudes down to 25–30 km (Engel et al., 2006; Huret et al., 2006; Funke et al., 2009). At NH
99 mid-latitudes, CO also exhibits significant variability during periods of planetary wave activity
100 associated with SSWs, when the polar vortex splits and displaces off the pole (Solomon et al.,
101 1985; Allen et al., 1999; Funke et al., 2009).

102 Recent atmospheric models are being extended up to 80–150 km and are used for the study
103 of SSWs (de la Torre et al., 2012; Chandran and Collins, 2014; Shepherd et al., 2014;
104 Limpasuvan et al., 2016; Newnham et al., 2016). For example, de la Torre et al. (2012) applied
105 the Whole Atmosphere Community Climate Model (WACCM) and Shepherd et al. (2014) used

106 the Canadian Middle Atmosphere Model (CMAM) for SSW modeling. The reference wind
107 profiles for the models are mainly retrieved from observations of the radiation of the
108 mesospheric ozone molecules, which allow robust measurements at altitudes up to of
109 approximately 65 km (e.g., Hagen et al., 2018). These data are generally consistent with the
110 most commonly used reanalysis products. However, there are still insufficient observations of
111 middle atmospheric winds at altitudes between 60 and 85 km made with a high vertical
112 resolution to verify atmospheric models and possible long-term trends (Keuer et al., 2007;
113 Hagen et al., 2018; Rüfenacht et al., 2018). This altitude range, where temperature generally
114 decreases with height, which causes inherent vertical instability, is situated below the winter
115 mesopause region at 95–100 km (e.g. Xu et al., 2009) and plays a significant role in the mass
116 and energy exchange between the stratosphere and the mesosphere (Shepherd et al., 2014;
117 Limpasuvan et al., 2016; Gardner, 2018).

118 Microwave radiometry is a ground-based technique that can provide vertical profiles of CO,
119 H_2O and O_3 atmospheric gases and wind data in the upper stratosphere and mesosphere
120 (Rüfenacht et al., 2012; Scheiben et al., 2012; Forkman et al., 2016). The upper stratosphere–
121 mesosphere zonal winds at the 30–85 km altitude region can be measured using the Doppler
122 shift between different observation directions in simultaneously measured spectra of transitions
123 lines of carbon monoxide at 115.3 GHz and ozone O_3 at 110.8 GHz (Rüfenacht et al., 2012;
124 Forkman et al., 2016). Due to high altitude CO residence region, the simultaneous zonal wind
125 measurements using both O_3 and CO provide independent data that extend the wind
126 measurement from the stratospheric to mesospheric altitudes, respectively (Forkman et al.,
127 2016; Piddyachiy et al., 2017).

128 The first ground-based microwave measurements of CO were made in the 1970s and they
129 confirmed theoretical estimations of the vertical CO profile (Waters et al., 1976; Goldsmith et
130 al., 1979). Since the 1990s, the ground-based microwave radiometers measuring CO have been
131 installed in the Northern Hemisphere at high and middle latitudes to provide measurements on
132 a regular basis. Microwave radiometers are operating in Onsala and Kiruna, Sweden, since
133 2008. The results are described in Hoffmann et al. (2011) and in Forkman et al. (2012). The
134 microwave radiometer operated in Bern, Switzerland since 2010 aims to contribute to the
135 significant gap that exists in the middle atmosphere between 40 and 70 km altitude for wind
136 data (Rüfenacht et al., 2012). In the Arctic, the O_3 , N_2O , HNO_3 , and CO spectra were recorded
137 using the Ground-Based Millimetre-wave Spectrometer GBMS (Muscati et al., 2007; Di Biagio
138 et al., 2010).

139 Since 2014, the microwave measuring system for CO observations has been operated in
140 Kharkiv, Ukraine (Piddyachiy et al., 2010; Piddyachiy et al., 2017). Microwave radiometer

141 measurements of CO are used to retrieve mesospheric winds nearby the mesopause region (70–
142 85 km). Methods deriving the wind speed from mesospheric CO measurements are based on
143 the determination of the CO and O₃ lines emission Doppler shift (Eriksson et al., 2011; Hagen
144 et al., 2018).

145 Our observations in February 2018 using the new microwave radiometer at the mid-latitude
146 Kharkiv station have recorded the mesospheric effects of a major SSW. In mid-February 2018,
147 the stratospheric polar vortex in the Arctic splitted into two sister vortices (Fig. 1), the zonal
148 wind reversed in the stratosphere–mesosphere from westerly to easterly and warm air
149 penetrated into the polar cap regions (Rao et al., 2018; Karpechko et al., 2018; Vargin and
150 Kiryushov, 2019). This caused large-scale disturbances in the middle atmosphere of the polar
151 and middle latitudes. The major SSW in 2018 is not yet widely discussed in publications (Rao
152 et al., 2018; Karpechko et al., 2018; Vargin and Kiryushov, 2019) and in this paper, we give a
153 detailed description of the observed mesospheric CO and zonal wind variations.

154 In Sect. 2, the microwave radiometer and data processing software are briefly described.
155 The SSW event in February 2018 is considered in Sect. 3. The effects of the SSW on mid-
156 latitude mesosphere–stratosphere conditions in the Ukraine longitudinal sector are presented in
157 Sect. 4. Discussion is given in Sect. 5 followed by conclusions in Sect. 6.

158

159

160 **2 Data and methods**

161

162 The microwave radiometer data set registered during the 2017/2018 winter campaign in
163 Kharkiv (50.0°N, 36.3°E) is used in this study to investigate local effects of the winter 2018
164 sudden stratospheric warming on the mesosphere and stratosphere. Since the ground-based
165 microwave measurements are spatially limited by instrument coverage, data on air temperature,
166 zonal wind [and](#) geopotential height were used from reanalyses and satellite databases to
167 interpret the CO profile and the zonal wind microwave observations and to describe the SSW
168 effects in the atmosphere of the surrounding mid-latitude region (30–40°E, 48–52°N).

169

170

171 **2.1 Microwave radiometer, method, and midlatitude data description**

172

173 The microwave radiometer (MWR) with high sensitivity, installed at Kharkiv, Ukraine, is
174 designed for continuous observations of the atmospheric CO profiles and zonal wind speed in
175 the mesosphere using emission lines at 115.3 GHz. The radiometer can continuously provide

176 vertical profiles up to the mesopause region during day and night, even in cloudy conditions
177 (Hagen et al., 2018). However, precipitation, such as strong rain or snow, can prevent the
178 measurements.

179 The receiver of the radiometer has the double-sideband noise temperature of 250 K at an
180 ambient temperature of 10°C (Piddyachiy et al., 2010; 2017). The radiometer was tested during
181 the 2014–2015 period for observation of the CO emission lines in the mesosphere over
182 Kharkiv. These tests proved the reliability of the receiver system, on which further details are
183 provided in Piddyachiy et al. (2017). Since 2015, the radiometer has been used for continuous
184 microwave measurements of CO profiles and mesosphere wind investigations. The first
185 observations of the atmospheric CO spectral lines over Kharkiv have confirmed seasonal
186 variations in the CO abundance (Piddyachiy et al., 2017). Operation of the MWR in a double-
187 sideband mode allows retrieval of wind speed from the Doppler shift of the CO line emission at
188 the 115.3 GHz. Two methods are used to determine wind speed. Firstly the observed line shape
189 is fitted by a Voigt profile and the center frequency is determined (Piddyachiy et al., 2017).
190 Secondly radiative transfer calculations for a horizontally layered atmosphere are used to
191 determine the wind profiles with the Qpack package, version 1.0.93 (Eriksson et al., 2005;
192 Eriksson et. al., 2011), which is specifically designed to work with the forward model of the
193 Atmospheric Radiative Transfer Simulator ARTS (Buehler et al., 2018;
194 <http://www.radiativetransfer.org/>). The results obtained by both methods were almost the same
195 within the error limits. In this paper, both methods were used and provided average values of
196 the zonal wind speed for altitudes of 70–85 km. The time interval of the data used here was
197 January 1 – March 31, 2018, which covers the main phases of the SSW 2018 event.

198

199

200 **2.2 Data from other sources**

201

202 In this study, daily datasets from ERA-Interim global atmospheric reanalysis of European
203 Centre for Medium-Range Weather Forecast (ECMWF; Dee et al., 2011) were downloaded
204 from ([https://www.ecmwf.int/en/forecasts/datasets/archive-datasets/reanalysis-datasets/era-
interim](https://www.ecmwf.int/en/forecasts/datasets/archive-datasets/reanalysis-datasets/era-interim)) and have been used for comparison with MWR observations. The ERA-Interim data
206 were used to create temperature and zonal wind velocity profiles and to calculate geopotential
207 height at the stratospheric pressure levels, in order to compare with the data measured over the
208 Kharkiv site. Aura Microwave Limb Sounder (MLS) measurements of the air temperature were
209 analyzed as well (Xu et al., 2009; <https://mls.jpl.nasa.gov/data/readers.php>; see details in the
210 Supplement).

211 Zonal wave amplitudes in geopotential height were analyzed using the National Oceanic and
212 Atmospheric Administration National Centers for Environmental Prediction, Global Data
213 Assimilation System–Climate Prediction Center (NOAA NCEP GDAS–CPC) data at
214 <https://www.cpc.ncep.noaa.gov/products/stratosphere/strat-trop/> and the MERRA-2 data from
215 the National Aeronautics and Space Administration Goddard Space Flight Center, Atmospheric
216 Chemistry and Dynamics Laboratory (NASA GFC ACDL) site at [https://acd-](https://acd-ext.gsfc.nasa.gov/Data_services/met/ann_data.html)
217 [ext.gsfc.nasa.gov/Data_services/met/ann_data.html](https://acd-ext.gsfc.nasa.gov/Data_services/met/ann_data.html). The detailed description of the data used
218 for analysis is given in the Supplement.

219

220

221 **3 Northern Hemisphere SSW effects**

222

223 Descending air masses are observed throughout the mesosphere and stratosphere of the winter
224 polar region (Orsolini et al., 2010; Chandran and Collins, 2014; Limpasuvan et al., 2016;
225 Zülicke et al., 2018). From Aura MLS vertical profiles, a layered descending sequence of
226 alternating cool and warm anomalies over the polar cap was observed in the 2017/2018 winter
227 (Fig. 2a). The SSW event in Fig. 2a is identified by the rapid warming in the stratosphere and
228 cooling in the mesosphere (upward arrow) starting from 10 February 2018 (left vertical line).

229 This event was preceded by progressively descending warm and cold anomalies that formed
230 in January (black and white dashed arrows, respectively). Oscillations in the intensity of the
231 anomalies indicate that they were formed under the influence of large amplitude planetary
232 waves of zonal wave numbers 1 and 2 (Fig. 2c–2e). From 1 January to 10 February (during 41
233 days), descending warm anomalies with a velocity $-850 \text{ m}\cdot\text{day}^{-1}$ were apparent in the
234 mesosphere and the upper stratosphere (75 to 40 km; black dashed arrow in Fig. 2a). Below the
235 warm anomaly, a cold anomaly descended between the upper and lower stratosphere (45 to 20
236 km) with velocity $-600 \text{ m}\cdot\text{day}^{-1}$ (white dashed arrow in Fig. 2a), while a cold mesospheric
237 anomaly in February–March descended with average velocity $-750 \text{ m}\cdot\text{day}^{-1}$ (white dotted
238 arrow in Fig. 2a). Our velocity estimates are similar to those of Salmi et al. (2011) who found
239 that mesospheric NO_x anomalies during the major SSW 2009 were transported from 80 to 55
240 km in about 40 days, i.e. with velocity $-600 \text{ m}\cdot\text{day}^{-1}$.

241 The splitting of the polar vortex (Fig. 1) and the zonal wind reversal (Fig. 2b) started at the
242 time of the wave 2 pulse on 10 February (Fig. 2d and dashed curve in Fig. 2e). Note that this is
243 close to the SSW timing in Rao et al. (2018) and Vargin and Kiryushov (2019), where the SSW
244 onset date was 11 February. As seen from Fig. 2c and solid curve in Fig. 2e, increasing wave 1
245 amplitude contributed to the destabilization of the polar vortex during January–early February

246 and to temperature and zonal wind oscillations in the mesosphere and stratosphere (Fig. 2a and
247 2b). These oscillations are usually associated with the propagation of planetary waves in the
248 stratosphere and mesosphere (Limpasuvan et al., 2016; Rüfenacht et al., 2016). As noted in an
249 earlier study (Manney et al., 2009; Rao et al., 2018), wave 1 amplitudes were also larger prior
250 to the SSW in 2009, suggesting a role of preconditioning. During 10–15 February, the easterly
251 zonal wind anomaly at the stratopause (about 1 hPa, ~50 km) increased to -60 m s^{-1} (Fig. 2b).
252 At the same time, warming in the polar stratosphere with the largest temperature anomaly of
253 about 20 K was observed between 25 and 45 km in the same time interval (upward arrow in
254 Fig. 2a). Both anomaly peaks are close in time to the wave 1 pulse after the SSW start (Fig. 2c
255 and 2e). The descending negative temperature anomaly in the mesosphere between 50 and 90
256 km persisted during and after the SSW and reached -15 K (dotted arrow in Fig. 2a).

257

258

259 **4 The local SSW effects over the midlatitude station**

260

261 **4.1 CO variability**

262

263 Local variability in the conditions of the atmosphere during the microwave measurements in
264 January–March 2018 at Kharkiv (50.0°N , 36.3°E) is shown in Figs. 3–6. The sharp changes
265 occurred in the 20-day interval from 10 February to 1 March coinciding with the SSW event
266 2018, as indicated by red vertical lines in Figs. 3, 5 and 6. At this time the polar vortex divided
267 into two parts producing two smaller vortices over the longitudinal sectors of North America
268 and Eurasia (Fig. 1). Due to the planetary wave influence (Fig. 2c–2e), the two sub-vortices
269 shifted zonally and meridionally, so that the SSW effects were observed not only in the polar
270 region but also in the middle latitudes (Fig. 4).

271 The CO molecule volume mixing ratio (VMR) near the mesopause at 75–80 km decreased
272 from 10 ppmv of background level to 4 ppmv on 19–21 February (Fig. 3a), when the sharp
273 vertical CO gradient at the lower edge of the CO layer near about 6 ppmv increased in height
274 by about 8 km (between 75 km and 83 km, thick part of the white curve in Fig. 3a). For
275 comparison, the pre- and post-SSW vertical variations of the 6-ppmv contour were observed in
276 a range 2–3 km (white curve in Fig. 3a). Moreover, similar variations in the zonal mean 6-
277 ppmv level are much weaker (yellow curve in Fig. 3e). This indicates that local and regional
278 mesosphere over the MWR site was disturbed by some source acted during the SSW, which is
279 identified below. We take here the 6-ppmv contour as a conditional lower edge of the CO layer
280 since the CO gradients sharply increase from $0.2\text{--}0.3 \text{ ppmv km}^{-1}$ in a 10-km layer below to

281 0.6–0.8 ppmv km^{-1} in a 10-km layer above (below and above the white curve in Fig. 3a). The
282 similar gradient change is a characteristic of the mesospheric CO profiles in boreal winter from
283 ground-based and satellite observations (Fig. 4 in Koo et al., 2017; Fig. 5 in Ryan et al., 2017).

284 The local mesospheric CO variability from the MWR observations over Kharkiv agrees
285 with regional one from the MLS data averaged over the adjacent area 47.5–52.5°N, 26–46°E
286 (Fig. 3b, the white curve for 6 ppmv). However, the zonal mean CO profiles in the same zone
287 do not show an anomalous decrease of the mesospheric CO during the SSW (yellow curve in
288 Fig. 3a, 3b and 3e).

289 Unlike the mesosphere, the CO descent and an increase in CO abundance is observed in
290 the stratosphere from both regional and zonal mean MLS data shortly after the SSW start
291 (contour 0.1 ppmv in Fig. 3d and 3g, respectively). The CO-rich air of 0.1–0.5 ppmv, which is
292 typical for the lower mesosphere (Fig. 3c) descended down to about 30 km (Fig. 3d and 3g), far
293 exceeding typical stratospheric CO mixing ratios on the order of about 0.01–0.02 ppmv (Engel
294 et al., 2006; Huret et al., 2006; Funke et al. 2009). The CO-rich stratospheric anomaly is close
295 in time to the wave 1 peak on 10–15 February (solid curve in Fig. 2e), that was observed
296 through the stratosphere down to the 30 km altitude (Fig. 2c).

297 Horizontal distributions of the CO VMR in the Northern Hemisphere at the stratospheric
298 and mesospheric altitudes in Fig. 4 suggest causes of the different CO variability in the
299 stratosphere and mesosphere in Fig. 3. The dynamical deformation, elongation, and
300 displacements of the polar vortex relative to the pole lead to temporal shifts between the low
301 and high CO amounts over the MWR site at Kharkiv (white circle in Fig. 4). The tendency of
302 the planetary wave westward tilt with altitude (dashed lines in Fig. 4, see also Supplemental
303 Figs. S1 and S2 for more details) also contributes to relative zonal shift between the
304 stratosphere and the mesosphere of the low/high CO over Kharkiv.

305 The observed decrease of the local CO in the mesosphere during the SSW (white curve in
306 Fig. 3a) is consistent with the regional data from the satellite observations (white curve in Fig.
307 3b). The decrease is due to the displacement of the CO-rich air to the west relative to Kharkiv
308 (white circle and contours outlined the CO-rich area in Fig. 4a–4c and 4e–4g). This is a result
309 of the dominance of easterlies during the SSW that led to placing of the CO-poor air over
310 Kharkiv with the lowest CO levels on 19–23 February (Fig. 4c and 4g) in correspondence with
311 the MWR (Fig. 3a) and MLS (Fig. 3b) measurements. Recovery to the westerly regime in early
312 March reversed the rotation of the vortex (2–6 March in Fig. 4d and 4h) and caused recovery of
313 high CO level over Kharkiv (since about 1st of March in Fig. 3a and 3b).

314 The polar vortex split influenced the local CO change in the middle stratosphere (Fig. 4m–
315 4o). The low CO level at ~30 km before the SSW start (Fig. 3d) is associated with the relatively

316 distant location of the CO-rich vortex from Kharkiv (Fig. 4m). The vortex split and easterly
317 circulation caused displacement of the small vortex fragment with the CO level higher than 0.1
318 ppmv to Kharkiv just at the SSW start (9–13 February in Fig. 4n) and corresponding sharp CO
319 increase over the Kharkiv region around 30-km altitude (contour 0.1 ppmv in a few days after
320 10 February in Fig. 3d). Vertical CO profiles in Fig. 3c and 3d show that downward penetration
321 of the mesospheric CO-rich air into the stratosphere took place around 10 February. As seen
322 from Fig. 4f, 4j, and 4n, the mesospheric CO-rich air appears to be contained inside the small
323 sub-vortex over Kharkiv. The large sub-vortex (Fig. 4n and 4o) contributed to the stratospheric
324 CO increase after 10 February in the zonal mean CO profile near 30 km (Fig. 3g). The two sub-
325 vortices in Fig. 4n and 4o provided a longer duration of the mesospheric intrusion in the zonal
326 mean (Fig. 3g) than a short-time influence of the single sub-vortex in regional data (Fig. 3d).

327 It should be noted that the lower edge of the mid-latitude CO-rich air descended in January
328 – mid-February (dashed lines in Fig. 3d and 3g) similarly to the temperature anomaly in the
329 polar region (Fig. 2a). Descent velocity was about -270 and -220 m·day $^{-1}$ in the case of the
330 regional and zonal mean data, respectively. This is a few times lower than in the vortex region,
331 nevertheless, it is in the range of the winter descent velocity noted above (Ryan et al., 2018).

332 Note also that the vortex split in the CO distribution can be identified only in the middle
333 and upper stratosphere (Fig. 4n and 4o and Fig. S1j and S1k), but not at the stratopause level
334 (Fig. 4j and 4k) and in the mesosphere (Fig. S2, second and third columns for 9–13 and 19–23
335 February 2018, respectively).

336

337

338 **4.2 Zonal wind variability**

339

340 The reversal of the local zonal wind estimated from the CO measurements at the Kharkiv
341 MWR site near the mesopause region was observed. The averaged wind velocity in the altitude
342 range 70–85 km changed between 10 m s $^{-1}$ and -10 m s $^{-1}$ around 10 February (Fig. 5a). After
343 the active phase of the SSW, the zonal wind [recovers](#) to the westerly wind and enhances to 20
344 m s $^{-1}$ reaching the highest velocity observed in January–March (Fig. 5a). This zonal wind peak
345 in early March is accompanied by the CO peak at 18 ppmv around 85 km that is also the
346 highest CO abundance over January–March (Fig. 3a). This is closely consistent with the MLS
347 measurements at the 86-km altitude: Kharkiv was located on the 16-ppmv contour in early
348 March (2–6 March in Fig. 4d).

349 During the SSW event, local zonal wind over the station became easterly between the lower
350 stratosphere and lower mesosphere (-30 m s $^{-1}$ up to -40 m s $^{-1}$, white contours in Fig. 5b). Note

351 that westerly zonal wind at the stratopause level (~ 50 km) in January 2018 (mid-winter, the
352 pre-SSW conditions) sometimes increased to more than 100 m s^{-1} (black contours in Fig. 5b).

353 The **recovery** of the local westerly wind in the upper mesosphere began in late February
354 (Fig. 5a) and later, in early March, in the lower mesosphere–stratosphere (Fig. 5b). The longer
355 persistence of the westerly anomaly in the stratosphere than at the stratopause level **is also** seen
356 in the polar region (Fig. 2b). This is a manifestation of the downward migration of the
357 circulation anomalies in the SSW recovery phase, **while** a near-instantaneous vertical coupling
358 is observed at the SSW start on 10 February (Fig. 2a–2d and Fig. 5).

361 **4.3 Temperature changes**

363 The MLS temperature profiles show that high temperature variability over the Kharkiv region
364 concentrated at the stratopause level, particularly before and during the SSW 2018 (Fig. 6). As
365 known, the SSW events are accompanied by polar stratopause descent to 30–40 km, by
366 stratopause breakdown and subsequent reformation at very high altitudes of about 70–80 km
367 (Manney et al., 2009; Chandran et al., 2011; Limpasuvan et al., 2016; Orsolini et al., 2017).
368 The midlatitude stratopause exhibits less sharp, but significant oscillations between 40 and 50
369 km in January–first half of February 2018 (dotted curve in Fig. 6) and the highest temperature
370 near -5°C after the SSW start on 12–13 February. The short-time stratopause elevation to the
371 lower-mesospheric altitude ~ 60 km was observed near 20 February, i.e. close in time to the
372 maximum elevation of the 6-ppmv CO level in the mesosphere (Fig. 3a and 3b). Note that the
373 wave 1 and wave 2 (Fig. 2c–2e), and zonal wind (Fig. 5) do not demonstrate strong anomalies
374 this time. The post-SSW stratopause stabilized at the 50-km altitude and warmed from about
375 -20°C to -10°C (Fig. 6b).

376 Similarly to the CO profile in Fig. 3, the zonal mean temperature variability is much lower
377 above the stratopause than the regional one (Fig. 6b and 6a, respectively). The stratosphere **is**
378 equally disturbed in both regional and zonal mean characteristics (Fig. 3d and 3g and Fig. 6a
379 and 6b). This difference may be associated with the influence of the splitted (non-splitted) polar
380 vortex in the stratosphere (mesosphere). The vortex fragments introduce higher local/regional
381 and zonal mean variability in the stratosphere; whereas the vortex region is more uniform in the
382 mesosphere (Fig. 4). That results in the weaker zonal mean variability.

383 During the SSW, the regional stratospheric temperature in Fig. 6a was warmer by $10\text{--}15^\circ\text{C}$
384 in comparison with the pre- and post-SSW temperature. This is about two times lower warming

385 than in the polar region (Fig. 2a) and about three times lower than it is typically observed
386 during the SSWs (see Section 1). It should be noted that this warm stratospheric anomaly in
387 Fig. 6a (contour -50°C) rapidly descended between the upper and lower stratosphere (dashed
388 arrow) in about 10 days. A similar tendency is seen in Fig. 6b from the zonal mean (contour $-$
389 55°C) but with a descent within a few days (arrow). So, the SSW start in the midlatitude
390 stratosphere [is not accompanied by](#) a near-instantaneous vertical coupling [as](#) observed in the
391 polar region (Fig. 2a–2d). Midlatitude stratospheric warming in February 2018 occurred with
392 increasing time lag between the upper and lower stratosphere.

393 As is known, upward propagation of the tropospheric planetary waves into the stratosphere
394 is limited in the easterly zonal wind (Charney and Drazin, 1961). In the changed state of a
395 zonal flow, the critical line for planetary waves (zero wind line) in the polar region descents in
396 a few days that looks like downward propagation of an anomaly from above (Matsuno, 1971;
397 Zhou et al., 2002). Possibly, this process may be delayed in the midlatitude, as seen from Fig. 6.
398

399 **5 Discussion**

400
401 The observations of the major SSW effects in February 2018 in the NH midlatitude mesosphere
402 by microwave radiometer at the Kharkiv site, Northern Ukraine (50.0°N , 36.3°E), have been
403 provided. The CO altitude profiles in the mesosphere have been measured by the MWR with
404 one-day time resolution. Using the CO molecule as a tracer, the wind speed has been retrieved
405 from the Doppler shift of the CO 115.3 GHz emission and the mesospheric winds reverse from
406 westerly to easterly below the winter mesopause region (70–85 km) has been detected. A few
407 ground-based observations in the mesosphere by the same method have been undertaken at
408 midlatitudes (Sect. 1). The zonal wind and CO profile variability during the major SSW were
409 compared with the daily zonal wind, temperature [and zonal wave 1/wave 2](#) datasets from the
410 MLS data, the ERA-Interim, and MERRA-2 reanalyses. The SSW started with the polar vortex
411 split around 10 February (Fig. 1), zonal wind reverse in the mesosphere and stratosphere (Fig.
412 2b and Fig. 5) and enhanced stratosphere warming and mesosphere cooling (Fig. 2a).
413

414 **5.1 Wave patterns and CO level**

415
416 As noted in Sect. 1, CO abundance in the extratropical mesosphere increases with latitude
417 toward the winter pole due to meridional transport. CO accumulation results in the formation of
418 the CO layer with the sharp vertical gradient at its lower edge (Solomon et al., 1985; Shepherd
419 et al., 2014). [Because of the horizontal CO gradient at the polar vortex edge, its split and](#)

420 displacement during the SSW cause a significant CO variability at the NH midlatitudes
421 (Solomon et al., 1985; Allen et al., 1999; Funke et al., 2009; Shepherd et al., 2014).

422 In Sect. 4a, based on the MWR observations, we have defined the lower CO edge at 6 ppmv
423 and this edge uplifted during the SSW by about 8 km (between 75 km and 83 km, thick part of
424 the white curve in Fig. 3a). This uplifting noticeably stands out against the pre- and post-SSW
425 variations of the 6-ppmv level occurring within 2–3 km (Fig. 4a). The MLS CO measurements
426 show similar variations in the 6-ppmv level over the Kharkiv region (white curve in Fig. 3b)
427 and their absence in the corresponding zonal mean (yellow curve in Fig. 3a, 3b, and 3e).

428 Mesospheric CO profile uplifting is usually associated with the stratopause elevation
429 during the SSW, when air, poor in CO, enters the mesospheric CO layer from below (Kvissel et
430 al., 2012; Shepherd et al., 2014). Similar ascending motions in the stratopause and mesopause
431 regions were observed in the 2013 SSW from nitric oxide (NO) and showed that the NO
432 contours deflected upwards throughout the mesosphere (Orsolini et al., 2017). Our analysis
433 reveals that the local CO profile variations during the SSW 2018 were closely associated with
434 the changes in the planetary wave patterns in the mesosphere.

435 The MLS CO distribution demonstrates how deformation, elongation (wave 2 effect) and
436 rotation of the CO-rich polar area influence the local CO level over Kharkiv (white circle with
437 respect to the CO contours in Fig. 4a–4h and Fig. S1). The highest elevation of the 6-ppmv CO
438 level in Fig. 3a and 3b corresponds to the lowest CO level over Kharkiv on 19–23 February,
439 when the most distant displacement of the CO contours 16 ppmv and 6 ppmv off the Kharkiv
440 location was observed (Fig. 4c and 4g, respectively; see also the third column in Fig. S1). As
441 known, the strong vertical CO gradient in the winter mesosphere is found at the higher altitudes
442 in the tropics than in the extratropics (Solomon et al., 1985; Allen et al., 1999; Garcia et al.,
443 2014). Then, poleward displacement of the low-latitude air masses is accompanied by the CO
444 abundance decrease and vertical CO gradient elevation at the middle latitudes, as it is observed
445 in Fig. 3a and 3b. A similar effect related to the wave 1 influence was observed during the
446 2003–2004 Arctic warming (Funke et al., 2009): the vortex has shifted from the pole toward the
447 western sector and mid-latitude air poor in CO filled the eastern sector (0–90°E) over 50–80°N
448 and even over the pole.

449 The results of Fig. 4 and Fig. S1 show that meridional displacements of the low-latitude,
450 CO-poor mesospheric air to the Kharkiv region occurred under the planetary wave influence
451 and caused the local CO profile variations in the SSW 2018 (Fig. 3a and 3b). These results,
452 thus, confirm that latitudinal displacements due to wave effects may dramatically affect the
453 local densities of the atmospheric species (Solomon et al., 1985). Figure 6a demonstrates that
454 the local stratopause elevation in February 2018 to about 60 km was relatively small in

455 comparison with the elevation that is characteristic for the polar region, up to 70–80 km
456 (Chandran et al., 2011; Tomikawa et al., 2012; Limpasuvan et al., 2016; Orsolini et al., 2010,
457 2017). No significant stratopause elevation was observed in the zonal mean for 47.5–52.5°N
458 (Fig. 6b). Therefore, the meridional (poleward) and zonal displacements of the CO-rich air
459 masses enclosed within the polar vortex (Solomon et al., 1985; Allen et al., 1999; Funke et al.,
460 2009) rather than stratopause elevation (Kvissel et al., 2012; Shepherd et al., 2014) may be
461 dominant cause of the CO profile uplift observed in the NH midlatitudes during the SSW 2018.

462 In March 2018, after the SSW, vertical CO profile has been re-established (Fig. 3a and 3b)
463 according to the recovery phase following the SSW (Shepherd et al., 2014; Limpasuvan et al.,
464 2016). In the MWR data, the SSW recovery phase in the mesosphere in early March started
465 with the short-term but anomalously high peaks in the local CO (Fig. 3a) and westerly wind
466 (Fig. 5a). These peaks reached the highest values in daily variations of CO and zonal wind over
467 the three months of the observations (January–March). By analogy with the low-CO episode in
468 February discussed above, the high-CO peak in early March 2018 caused by change in the
469 vortex shape [and the return](#) of the CO-rich vortex edge region to the Kharkiv location (compare
470 2–6 March in Fig. 4d and 4h with 19–23 February in Fig. 4c and 4g; see also the same dates in
471 Fig. S2).

472 Wind measurements using the CO layer provide a further means to evaluate the validity of
473 the modeled winds. Furthermore, by combining the measurements with ray tracing of gravity
474 wave propagation (e.g. Kogure et al., 2018), this type of measurement may provide specific
475 insights into wave-mean flow interactions, particularly where local temperature inversions alter
476 gravity wave filtering (Hocke et al., 2018; Fritts et al., 2018).

477

478

479 **5.2 Descent of the midlatitude stratospheric anomalies**

480

481 Alternating altitudinal sequence of warm and cool anomalies progressively descended through
482 the mesosphere and stratosphere of the polar region was observed in January–March 2018 (Fig.
483 2a) in consistency with many observations (Zhou et al., 2002; Orsolini et al., 2010; Shepherd et
484 al., 2014; de Wit et al., 2014; Zülicke et al., 2018). The warm anomaly sharply intensified in the
485 stratosphere between 20 and 50 km with simultaneous strong cooling in the mesosphere in the
486 active phase of SSW since 10 February (vertical arrow in Fig. 2a). Unlike this, the midlatitude
487 temperature anomalies do not show the similar vertical arrangement and regular descent with
488 respect to the same mean climatology 2005–2017 (Fig. [S3](#)).

489 During the SSW of 2018, the upper (lower) stratosphere over the Kharkiv region was cooler
490 (warmer) up to 20°C (10°C) than climatological mean with stepwise descent relative to the pre-
491 SSW one (Fig. S3a). However, excluding unstable anomalies at different altitudes, the air
492 temperature through the mesosphere and stratosphere was close to the climatology during most
493 of the time in January–March 2018 (light blue in Fig. S3a). The zonal mean temperature
494 anomalies in Fig. S3b show steady warming of the air in the stratosphere and lower mesosphere
495 and distinct tendency for the anomaly to descend between about 40 km and 20 km during the
496 SSW (20 days, $\sim 1 \text{ km} \cdot \text{day}^{-1}$). It could be concluded that the temperature anomaly profile
497 observed in the NH midlatitudes may vary in time depending on the observing location and
498 individual SSW event and, thus, differ from climatologically warm (cold) stratospheric
499 (mesospheric) anomaly typical for the SSWs in the NH polar region (e.g. Chandran and
500 Collins, 2014; their Fig. 1g).

501 The CO profiles in Fig. 3 demonstrate opposite tendencies in the vertical shift of the CO-
502 rich air in the NH midlatitudes. The CO descent in the stratosphere occurred during January–
503 February with velocities of about 270 and 220 $\text{m} \cdot \text{day}^{-1}$ in a case of the regional and zonal mean
504 data, respectively (Fig. 3d and 3g). In general, this is in a range of the winter descent velocities
505 observed in the polar vortex (Funke et al., 2009; Salmi et al., 2011; Ryan et al., 2018), however,
506 a few times lower than in the polar vortex in the winter 2017–2018 (Fig. 2a). The deepest
507 penetration of the mesospheric CO levels (0.1–0.5 ppmv) to ~ 30 km was observed immediately
508 after the SSW onset (Fig. 3d and 3g). Although this coincides with the peaks in the wave 1 and
509 wave 2 amplitudes (Fig. 2e), the main reason in the CO increase in the stratosphere over
510 Kharkiv is the location of the small sub-vortex of the split polar vortex (9–13 February, Fig.
511 4n).

512 The MLS CO maps in Fig. 4 show that the high CO amount is concentrated inside the polar
513 vortex and its fragments after splitting. This is a result of meridional and downward transport of
514 CO that is strongest in the winter polar vortex (Rinsland et al., 1999; Manney et al., 2009;
515 Kvissel et al., 2012; Shepherd et al., 2014). Before (4–8 February), during (19–23 February)
516 and after (2–6 March) the SSW, Kharkiv was outside the stratospheric vortex/sub-vortices edge
517 (Fig. 4m, 4o and 4p, respectively) and the CO amount was at low level typical for the
518 midlatitude stratosphere (of about 0.01–0.02 ppmv; Engel et al., 2006; Huret et al., 2006; Funke
519 et al. 2009). Descent of the 0.1-ppmv contour marked by dashed lines in Fig. 3d and 3g is
520 observed due to the episodic shift of the vortex edge toward the Kharkiv region or to the
521 corresponding zone 47.5–52.5°N, respectively.

522 Figure 4 demonstrates that the CO amount inside the polar vortex or its fragments is much
523 higher than in the surrounding area not only in the mesosphere but also in the stratosphere. This
524 leads to the possibility of the enhanced CO appearance even in the stratosphere at about 25–30
525 km (Engel et al., 2006; Huret et al., 2006; Funke et al., 2009). By analogy, the vortex edge shift
526 beyond the Kharkiv region (Fig. 4c and 4g) resulted in lowering of the regional CO mixing
527 ratios in the mesosphere **consistent with** both ground-based and satellite observations (Fig. 3a
528 and 3b, respectively). Meridional structure of the mesospheric CO (Sect. 1) provided the uplift
529 of the 6-ppmv level during the SSW relative to pre- and post-SSW levels (Fig. 3a and 3b).

530

531 **6 Conclusions**

532

533 The impact of a major sudden stratospheric warming in February 2018 on the mid-latitude
534 mesosphere was investigated using microwave radiometer measurements in Kharkiv, Ukraine
535 (50.0°N, 36.3°E). The zonal wind reversal has been revealed below the winter mesopause
536 region at 70–85 km altitudes during the SSW using the CO profiles. The reverse of the
537 mesospheric westerly from about 10 m s^{-1} to easterly wind about -10 m s^{-1} around 10 February
538 has been documented. The data from the ERA-Interim and MERRA-2 reanalyses and the Aura
539 MLS temperature profiles have been used for the analysis of stratosphere–mesosphere behavior
540 under the SSW conditions. Our local microwave observations in the NH midlatitude combined
541 with the reanalysis data show wide ranges of daily variability in CO, zonal wind and
542 temperature in the mesosphere and stratosphere during the SSW 2018.

543 **Among the most striking SSW manifestations over the midlatitude station in February**
544 **2018, there were (i) zonal wind reversal throughout the mesosphere–stratosphere, (ii)**
545 **oscillations in the vertical profiles of CO, zonal wind and temperature, (iii) descent of the**
546 **stratospheric CO and temperature anomalies on the time scale of days to months, (iv) wave 2**
547 **peak at the vortex split date and (v) strong mesospheric CO and westerly peaks at the start of**
548 **the SSW recovery phase. Generally, the midlatitude SSW effects are known from many event**
549 **analyses and in most cases they are associated with zonal asymmetry and polar vortex split and**
550 **displacements relative to the pole (Solomon et al., 1985; Allen et al., 1999; Yuan et al., 2012;**
551 **Chandran and Collins, 2014). Our results show that the local midlatitude atmosphere variability**
552 **in the SSW 2018 includes both the large-scale changes in the zonal circulation and temperature**
553 **typical for the SSWs and local evolution of the altitude-dependent planetary wave patterns in**
554 **the individual vortex split event.**

555 The observed local CO variability can be explained mainly by horizontal air mass
556 redistribution due to planetary wave activity with the replacement of the CO-rich air by CO-

557 poor air and vice versa, in agreement with other studies. The MLS CO fields show that the CO-
558 rich air masses are enclosed within the polar vortex. Horizontal (meridional and zonal)
559 displacements of the edge of the vortex or vortex fragments relative to the ground-based
560 midlatitude station may be a dominant cause of the observed CO profile variations during the
561 SSW 2018. The small sub-vortex located over the station at the SSW start caused the
562 appearance of the enhanced CO level not only in the mesosphere but also in the stratosphere at
563 about 30 km. This indicates that the polar vortex contains the CO-rich air masses with much
564 higher CO amount [than](#) in the surrounding area and this takes place over the stratosphere–
565 mesosphere altitude range.

566 Microwave observations show that sharp altitudinal CO gradient below the mesopause
567 could be used to define the lower edge of the CO layer and to evaluate oscillation and
568 significant elevation of the lower CO edge during the SSW and its trend on a seasonal time
569 scale. The presented results of microwave measurements of CO and zonal wind in the
570 midlatitude mesosphere at 70–85 km altitudes, which is still not adequately covered by ground-
571 based observations (Hagen et al., 2018; Rüfenacht et al., 2018), are suitable for evaluating and
572 potentially improving atmospheric models. Simulations show that planetary wave forcing by
573 westward propagating wave 1 dominates between 40 and 80 km in the winter polar region
574 during the SSW (Limpasuvan et al., 2016). Our spectral analysis reveals that the westward
575 wave 1 during the SSW 2018 is a dominant wave component through the midlatitude upper
576 stratosphere–mesosphere. Instability of the westward polar jet suggested in previous studies
577 (e.g. Limpasuvan et al., 2016) should be analyzed in the context of the westward wave 1
578 generation in the midlatitude upper stratosphere–mesosphere.

579 Our observation of variability of the CO layer during the SSW deserves further study,
580 particularly in relation to the implications for modelling of wave dynamics and vertical
581 coupling (Ern et al., 2016; Martineau et al., 2018) and chemical processes (Garcia et al., 2014)
582 in the mesosphere.

583

584

585 *Conflict of Interest.* The authors declare that the research was conducted in the absence of any
586 commercial or financial relationships that could be construed as a potential conflict of interest.

587

588 *Author contributions.* GM coordinated and led the efforts for this manuscript. VS initiated the
589 microwave measurements during the SSW event in Kharkiv. VS, DS, VM and AA developed
590 equipment and provided microwave measurements with data processing by AP and DS. GM,

591 VS, YW, OE, AK, and AG analyzed the results and provided interpretation. GM, OE, AK, VS,
592 and WH wrote the paper with input from all authors.

593

594

595 *Acknowledgments.* This work was supported in part by the Institute of Radio Astronomy of the
596 National Academy of Sciences of Ukraine; by Taras Shevchenko National University of Kyiv,
597 project 19BF051-08; by the College of Physics, International Center of Future Science, Jilin
598 University, China. The microwave radiometer data have been processed using ARTS and
599 Qpack software packages (<http://www.radiativetransfer.org/>). Daily datasets from ERA-Interim
600 reanalysis of European Centre for Medium-Range Weather Forecast (ECMWF) were
601 downloaded from <https://www.ecmwf.int/en/forecasts/datasets/archive-datasets/reanalysis-datasets/era-interim>. The Aura Microwave Limb Sounder (MLS) measurements of air
602 temperature and CO were obtained from <https://mls.jpl.nasa.gov/data/readers.php>. Zonal waves
603 were analyzed using the National Oceanic and Atmospheric Administration National Centers
604 for Environmental Prediction, Global Data Assimilation System–Climate Prediction Center
605 (NOAA NCEP GDAS–CPC) data at
606 <https://www.cpc.ncep.noaa.gov/products/stratosphere/strat-trop/> and the MERRA-2 data from
607 the National Aeronautics and Space Administration Goddard Space Flight Center, Atmospheric
608 Chemistry and Dynamics Laboratory (NASA GFC ACDL) site at https://acd-ext.gsfc.nasa.gov/Data_services/met/ann_data.html. Authors thank the two anonymous
609 reviewers for their valuable comments and useful suggestions.

610

611

612

613

614 **References**

615

616 Alexander, S. P. and Shepherd, M. G.: Planetary wave activity in the polar lower stratosphere,
617 *Atmos. Chem. Phys.*, 10, 707–718, <https://doi.org/10.5194/acp-10-707-2010>, 2010.

618 Allen, D. R., Stanford, J. L., López-Valverde, M. A., Nakamura, N., Lary, D. J., Douglass, A.
619 R., Cerniglia, M. C., Remedios, J. J., and Taylor F. W.: Observations of middle atmosphere
620 CO from the UARS ISAMS during the early northern winter 1991/92, *J. Atmos. Sci.*, 56,
621 563–583, 1999.

622 Baldwin, M. P. and Dunkerton, T. J.: Stratospheric harbingers of anomalous weather regimes,
623 *Science*, 294, 581–584, doi:10.1126/science.1063315, 2001.

624 Buehler, S. A., Mendrok, J., Eriksson, P., Perrin, A., Larsson, R., and Lemke, O.: ARTS, the
625 atmospheric radiative transfer simulator – version 2.2, the planetary toolbox edition,
626 *Geosci. Model Dev.*, 11, 1537–1556, doi:10.5194/gmd-11-1537-2018, 2018.

627 Butler, A. H. and Gerber, E. P. Optimizing the definition of a sudden stratospheric warming,
628 *J. Climate*, 31, 2337–2344, doi:10.1175/JCLI-D-17-0648.1, 2018.

629 Butler, A. H., Seidel, D. J., Hardiman, S. C., Butchart, N., Birner, T., and Match, A.: Defining
630 sudden stratospheric warmings, *Bull. Amer. Meteor. Soc.*, 96, 1913–1928,
631 doi:10.1175/bams-d-13-00173.1, 2015.

632 Butler, A. H., Sjoberg, J. P., Seidel, D. J., and Rosenlof, K. H.: A sudden stratospheric warming
633 compendium, *Earth Syst. Sci. Data*, 9, 63–76, doi:10.5194/essd-9-63-2017, 2017.

634 Chandran, A. and Collins, R. L.: Stratospheric sudden warming effects on winds and
635 temperature in the middle atmosphere at middle and low latitudes: a study using WACCM,
636 *Ann. Geophys.*, 32, 859–874, doi:10.5194/angeo-32-859-2014, 2014.

637 Chandran, A., Collins, R. L., Garcia, R. R., and Marsh, D. R.: A case study of an elevated
638 stratopause generated in the Whole Atmosphere Community Climate Model, *Geophys. Res.*
639 *Lett.*, 38, L08804, doi:10.1029/2010GL046566, 2011.

640 Charlton, A. J. and Polvani, L. M.: A new look at stratospheric sudden warmings. Part I:
641 Climatology and modeling benchmarks. *J. Climate*, 20, 449–469, 2007. doi:10.1175/JCLI-
642 D-11-00348.1

643 Charney, J. G. and Drazin, P. G.: Propagation of planetary-scale disturbances from the lower
644 into the upper atmosphere, *J. Geophys. Res.*, 66, 83–109, doi:10.1029/JZ066i001p00083,
645 1961.

646 Dee, D. P., Uppala, S. M., Simmons, A. J., Berrisford, P., Poli, P., Kobayashi, S., Andrae, U.,
647 Balmaseda, M. A., Balsamo, G., Bauer, P., Bechtold, P., Beljaars, A. C. M., van de Berg, L.,
648 Bidlot, J., Bormann, N., Delsol, C., Dragani, R., Fuentes, M., Geer, A. J., Haimberger, L.,
649 Healy, S. B., Hersbach, H., Hólm, E. V., Isaksen, L., Källberg, P., Köhler, M., Matricardi,
650 M., McNally, A. P., Monge-Sanz, B. M., Morcrette, J.-J., Park, B. K., Peubey, C., de
651 Rosnay, P., Tavolato, C., Thépaut, J.-N., and Vitart, F.: The ERA-Interim reanalysis:
652 configuration and performance of the data assimilation system, *Q. J. Roy. Meteor. Soc.*,
653 137, 553–597, doi:10.1002/qj.828, 2011.

654 de la Torre, L., Garcia, R. R., Barriopedro, D., and Chandran, A.: Climatology and
655 characteristics of stratospheric sudden warmings in the Whole Atmosphere Community
656 Climate Model, *J. Geophys. Res.*, 117, D04110, doi:10.1029/2011JD016840, 2012.

657 de Wit, R. J., Hibbins, R. E., Espy, P. J., Orsolini, Y. J., Limpasuvan, V., and Kinnison, D. E.:
658 Observations of gravity wave forcing of the mesopause region during the January 2013

659 major Sudden Stratospheric Warming, *Geophys. Res. Lett.*, 41, 4745–4752,
660 doi:10.1002/2014GL060501, 2014.

661 Di Biagio, C., Muscari, G., di Sarra, A., de Zafra, R. L., Eriksen, P., Fiocco, G., Fiorucci, I., and
662 Fuà, D.: Evolution of temperature, O₃, CO, and N₂O profiles during the exceptional 2009
663 Arctic major stratospheric warming as observed by lidar and millimeter wave spectroscopy
664 at Thule (76.5N, 68.8W), Greenland, *J. Geophys. Res.*, 115, D24315,
665 doi:10.1029/2010JD014070, 2010.

666 Engel, A., Möbius, T., Haase, H.-P., Bönisch, H., Wetter, T., Schmidt, U., Levin, I., Reddmann,
667 T., Oelhaf, H., Wetzel, G., Grunow, K., Huret, N., and Pirre, M.: Observation of
668 mesospheric air inside the arctic stratospheric polar vortex in early 2003, *Atmos. Chem.*
669 *Phys.*, 6, 267–282, doi:10.5194/acp-6-267-2006, 2006.

670 Eriksson, P., Buehler, S. A., Davis, C. P., Emde, C., and Lemke, O.: ARTS, the atmospheric
671 radiative transfer simulator, version 2, *J. Quant. Spectrosc. Radiat. Transfer*, 112, 1551–
672 1558, doi: 10.1016/j.jqsrt.2011.03.001, 2011.

673 Eriksson, P., Jiménez, C., and Buehler, S. A.: Qpack, a tool for instrument simulation and
674 retrieval work, *J. Quant. Spectrosc. Radiat. Transfer*, 91, 47–64, doi:
675 10.1016/j.jqsrt.2004.05.050, 2005.

676 Ern, M., Trinh, Q. T., Kaufmann, M., Krisch, I., Preusse, P., UngermaNN, J., Zhu, Y., Gille, J.
677 C., Mlynczak, M. G., Russell III, J. M., Schwartz, M. J., and Riese, M.: Satellite
678 observations of middle atmosphere gravity wave absolute momentum flux and of its
679 vertical gradient during recent stratospheric warmings, *Atmos. Chem. Phys.*, 16, 9983–
680 10019, <https://doi.org/10.5194/acp-16-9983-2016>, 2016.

681 Feng, W., Kaifler, B., Marsh, D. R., Höffner, J., Hoppe, U.-P., Williams, B. P., and Plane, J. M.
682 C.: Impacts of a sudden stratospheric warming on the mesospheric metal layers, *J. Atmos.*
683 *Solar-Terr. Phys.*, 162, 162–171, 2017.

684 Forkman, P., Christensen, O. M., Eriksson, P., Urban, J., and Funke, B.: Six years of
685 mesospheric CO estimated from ground-based frequency-switched microwave radiometry
686 at 57° N compared with satellite instruments, *Atmos. Meas. Tech.*, 5, 2827–2841, doi:
687 10.5194/amt-5-2827-2012, 2012.

688 Forkman, P., Christensen, O. M., Eriksson, P., Billade, B., Vassilev, V., and Shulga, V. M.: A
689 compact receiver system for simultaneous measurements of mesospheric CO and O₃,
690 *Geosci. Instrum. Method. Data Syst.*, 5, 27–44, doi:10.5194/gi-5-27-2016, 2016.

691 Fritts, D. C., Laughman, B., Wang, L., Lund, T. S., and Collins, R. L.: Gravity wave dynamics
692 in a mesospheric inversion layer: 1. Reflection, trapping, and instability dynamics, *J.*
693 *Geophys. Res.-Atmos.*, 123, 626–648, <https://doi.org/10.1002/2017JD027440>, 2018.

694 Funke, B., López-Puertas, M., García-Comas, M., Stiller, G. P., von Clarmann, T., Höpfner, M.,
695 Glatthor, N., Grabowski, U., Kellmann, S., and Linden, A.: Carbon monoxide distributions
696 from the upper troposphere to the mesosphere inferred from 4.7 μ m non-local thermal
697 equilibrium emissions measured by MIPAS on Envisat, *Atmos. Chem. Phys.*, 9, 2387–2411,
698 <https://doi.org/10.5194/acp-9-2387-2009>, 2009.

699 García, R. R., López-Puertas, M., Funke, B., Marsh, D. R., Kinnison, D. E., Smith, A. K., and
700 González-Galindo, F.: On the distribution of CO₂ and CO in the mesosphere and lower
701 thermosphere, *J. Geophys. Res.-Atmos.*, 119, 5700–5718, doi:10.1002/2013JD021208,
702 2014.

703 Gardner, C. S.: Role of wave induced diffusion and energy flux in the vertical transport of
704 atmospheric constituents in the mesopause region, *J. Geophys. Res.-Atmos.*, 123, 6581–
705 6604, <https://doi.org/10.1029/2018JD028359>, 2018.

706 Goldsmith, P. F., Litvak, M. M., Plambeck, R. L., and Williams, D. R.: Carbon monoxide
707 mixing ratios in the mesosphere derived from ground-based microwave measurements, *J.*
708 *Geophys. Res.*, 84, 416–418, 1979.

709 Hagen, J., Murk, A., Rüfenacht, R., Khaykin, S., Hauchecorne, A., and Kämpfer, N.: WIRA-C:
710 a compact 142-GHz-radiometer for continuous middle-atmospheric wind measurements,
711 *Atmos. Meas. Tech.*, 11, 5007–5024, doi: 10.5194/amt-11-5007-2018, 2018.

712 Hocke, K., Lainer, M., Bernet, L., and Kämpfer, N.: Mesospheric inversion layers at mid-
713 latitudes and coincident changes of ozone, water vapour and horizontal wind in the Middle
714 Atmosphere, *Atmosphere*, 9, 171, <https://doi.org/10.3390/atmos9050171>, 2018.

715 Hoffmann, C. G., Raffalski, U., Palm, M., Funke, B., Golchert, S. H. W., Hochschild, G., and
716 Notholt, J.: Observation of strato-mesospheric CO above Kiruna with ground-based
717 microwave radiometry – retrieval and satellite comparison, *Atmos. Meas. Tech.*, 4, 2389–
718 2408, <https://doi.org/10.5194/amt-4-2389-2011>, 2011.

719 Hu, J., Ren, R., and Xu, H.: Occurrence of winter stratospheric sudden warming events and the
720 seasonal timing of spring stratospheric final warming, *J. Atmos. Sci.*, 71, 2319–2334,
721 doi:10.1175/JAS-D-13-0349.1, 2014.

722 Huret, N., Pirre, M., Hauchecorne, A., Robert, C., and Catoire, V.: On the vertical structure of
723 the stratosphere at midlatitudes during the first stage of the polar vortex formation and in
724 the polar region in the presence of a large mesospheric descent, *J. Geophys. Res.*, 111,
725 D06111, doi:10.1029/2005JD006102, 2006.

726 Karpechko, A. Yu., Charlton-Perez, A., Balmaseda, M., Tyrrell, N., and Vitart, F.: Predicting
727 sudden stratospheric warming 2018 and its climate impacts with a multimodel ensemble,
728 *Geophys. Res. Lett.*, 24, 13538–13546, <https://doi.org/10.1029/2018GL081091>, 2018.

729 Keuer, D., Hoffmann, P., Singer, W., and Bremer, J.: Long-term variations of the mesospheric
730 wind field at mid-latitudes, *Ann. Geophys.*, 25, 1779–1790, doi:10.5194/angeo-25-1779-
731 2007, 2007.

732 Kogure, M., Nakamura, T., Ejiri, M. K., Nishiyama, T., Tomikawa, Y., and Tsutsumi, M.:
733 Effects of horizontal wind structure on a gravity wave event in the middle atmosphere over
734 Syowa (69°S, 40°E), the Antarctic, *Geophys. Res. Lett.*, 45, 5151–5157.
735 <https://doi.org/10.1029/2018GL078264>, 2018.

736 Koo, J.-H., Walker, K. A., Jones, A., Sheese, P. E., Boone, C. D., Bernath, P. F., and Manney, G.
737 L.: Global climatology based on the ACE-FTS version 3.5 dataset: Addition of mesospheric
738 levels and carbon-containing species in the UTLS, *J. Quant. Spectrosc. Radiat. Transfer*,
739 186, 52–62, doi:10.1016/j.jqsrt.2016.07.003, 2017.

740 Kuttippurath, J. and Nikulin, G.: A comparative study of the major sudden stratospheric
741 warmings in the Arctic winters 2003/2004–2009/2010, *Atmos. Chem. Phys.*, 12, 8115–
742 8129, <https://doi.org/10.5194/acp-12-8115-2012>, 2012.

743 Kvissel, O. K., Orsolini, Y. J., Stordal, F., Limpasuvan, V., Richter, J., and Marsh, D. R.:
744 Mesospheric intrusion and anomalous chemistry during and after a major stratospheric
745 sudden warming, *J. Atmos. Solar-Terr. Phys.*, 78–79, 116–124,
746 doi:10.1016/j.jastp.2011.08.015, 2012.

747 Limpasuvan, V., Orsolini, Y. J., Chandran, A., Garcia, R. R., and Smith, A. K.: On the
748 composite response of the MLT to major sudden stratospheric warming events with
749 elevated stratopause, *J. Geophys. Res.-Atmos.*, 121, 4518–4537,
750 doi:10.1002/2015JD024401, 2016.

751 Manney, G. L., Schwartz, M. J., Krüger, K., Santee, M. L., Pawson, S., Lee, J. N., Daffer, W.
752 H., Fuller, R. A., and Livesey, N. J.: Aura Microwave Limb Sounder observations of
753 dynamics and transport during the record-breaking 2009 Arctic stratospheric major
754 warming, *Geophys. Res. Lett.*, 36, L12815, doi:10.1029/2009GL038586, 2009.

755 Martineau, P., Son, S.-W., Taguchi, M., and Butler, A. H.: A comparison of the momentum
756 budget in reanalysis datasets during sudden stratospheric warming events, *Atmos. Chem.
757 Phys.*, 18, 7169–7187, <https://doi.org/10.5194/acp-18-7169-2018>, 2018.

758 Matsuno, T.: A dynamical model of the stratospheric sudden warming, *J. Atmos. Sci.*, 28,
759 1479–1494, [https://doi.org/10.1175/1520-0469\(1971\)028<1479:ADMOTS>2.0.CO;2](https://doi.org/10.1175/1520-0469(1971)028<1479:ADMOTS>2.0.CO;2),
760 1971.

761 Muscari, G., di Sarra, A., de Zafra, R. L., Lucci, F., Baordo, F., Angelini, F., and Fiocco, G.:
762 Middle atmospheric O₃, CO, N₂O, HNO₃, and temperature profiles during the warm Arctic
763 winter 2001–2002, *J. Geophys. Res.*, 112, D14304, doi:10.1029/2006JD007849, 2007.

764 Newnham, D. A., Ford, G. P., Moffat-Griffin, T., and Pumphrey, H. C.: Simulation study for
765 measurement of horizontal wind profiles in the polar stratosphere and mesosphere using
766 ground-based observations of ozone and carbon monoxide lines in the 230–250 GHz
767 region, *Atmos. Meas. Tech.*, 9, 3309–3323, doi:10.5194/amt-9-3309-2016, 2016.

768 Orsolini, Y. J., Limpasuvan, V., Pérot, K., Espy, P., Hibbins, R., Lossow, S., Larsson, K. R., and
769 Murtagh, D.: Modelling the descent of nitric oxide during the elevated stratopause event of
770 January 2013, *J. Atmos. Solar-Terr. Phys.*, 155, 50–61, doi:10.1016/j.jastp.2017.01.006,
771 2017.

772 Orsolini, Y. J., Urban, J., Murtagh, D. P., Lossow, S., and Limpasuvan, V.: Descent from the
773 polar mesosphere and anomalously high stratopause observed in 8 years of water vapor and
774 temperature satellite observations by the Odin Sub-Millimeter Radiometer, *J. Geophys.*
775 *Res.*, 115, D12305, doi:10.1029/2009JD013501, 2010.

776 Pedatella, N. M., Chau, J. L., Schmidt, H., Goncharenko, L. P., Stolle, C., Hocke, K., Harvey,
777 V. L., Funke, B., and Siddiqui, T. A.: How sudden stratospheric warming affects the whole
778 atmosphere, *Eos*, 99, <https://doi.org/10.1029/2018EO092441>, 2018.

779 Piddyachiy, V., Shulga, V., Myshenko, V., Korolev, A., Antyufeyev, O., Shulga, D., and
780 Forkman, P.: Microwave radiometer for spectral observations of mesospheric carbon
781 monoxide at 115 GHz over Kharkiv, Ukraine, *J. Infrared Milli. Terahz. Waves*, 38, 292–
782 302, doi:10.1007/s10762-016-0334-1, 2017.

783 Piddyachiy, V. I., Shulga, V. M., Myshenko, V. V., Korolev, A. M., Myshenko, A. V.,
784 Antyufeyev, A. V., Poladich, A. V., and Shkodin, V. I.: 3-mm wave spectroradiometer for
785 studies of atmospheric trace gases, *Radiophys. Quantum El.*, 53(5-6), 326–333.
786 <https://doi.org/10.1007/s11141-010-9231-y>, 2010.

787 Rao, J., Ren, R.-C., Chen, H., Liu, X., Yu, Y., and Yang, Y.: Sub-seasonal to seasonal hindcasts
788 of stratospheric sudden warming by BCC_CSM1.1(m): A comparison with ECMWF, *Adv.*
789 *Atmos. Sci.*, 36, 479–494, doi:10.1007/s00376-018-8165-8, 2019.

790 Rao, J., Ren, R., Chen, H., Yu, Yu., and Zhou, Y.: The stratospheric sudden warming event in
791 February 2018 and its prediction by a climate system model, *J. Geophys. Res.-Atmos.*, 123,
792 13332–13345, doi:10.1029/2018JD028908, 2018.

793 Rinsland, C. P., Salawitch, R. J., Gunson, M. R., Solomon, S., Zander, R., Mahieu, E.,
794 Goldman, A., Newchurch, M. J., Irion, F. W., and Chang, A. Y.: Polar stratospheric descent
795 of NO_y and CO and Arctic denitrification during winter 1992–1993, *J. Geophys. Res.*, 104,
796 1847–1861, 1999.

797 Rüfenacht, R., Baumgarten, G., Hildebrand, J., Schranz, F., Matthias, V., Stober, G., Lübken, F.-
798 J., and Kämpfer, N.: Intercomparison of middle-atmospheric wind in observations and

799 models, *Atmos. Meas. Tech.*, 11, 1971–1987, <https://doi.org/10.5194/amt-11-1971-2018>,
800 2018.

801 Rüfenacht, R., Hocke, K., and Kämpfer, N.: First continuous ground-based observations of
802 long period oscillations in the vertically resolved wind field of the stratosphere and
803 mesosphere, *Atmos. Chem. Phys.*, 16, 4915–4925, <https://doi.org/10.5194/acp-16-4915-2016>, 2016.

805 Rüfenacht, R., Kämpfer, N., and Murk, A.: First middle-atmospheric zonal wind profile
806 measurements with a new ground-based microwave Doppler-spectroradiometer, *Atmos.*
807 *Meas. Tech.*, 5, 2647–2659, doi:10.5194/amt-5-2647-2012, 2012.

808 Ryan, N. J., Kinnison, D. E., Garcia, R. R., Hoffmann, C. G., Palm, M., Raffalski, U., and
809 Notholt, J.: Assessing the ability to derive rates of polar middle-atmospheric descent using
810 trace gas measurements from remote sensors, *Atmos. Chem. Phys.*, 18, 1457–1474,
811 <https://doi.org/10.5194/acp-18-1457-2018>, 2018.

812 Ryan, N. J., Palm, M., Raffalski, U., Larsson, R., Manney, G., Millán, L., and Notholt, J.:
813 Strato-mesospheric carbon monoxide profiles above Kiruna, Sweden (67.8°N, 20.4°E),
814 since 2008, *Earth Syst. Sci. Data*, 9, 77–89, doi:10.5194/essd-9-77-2017, 2017.

815 Salmi, S. M., Verronen, P. T., Thölix, L., Kyrölä, E., Backman, L., Karpechko, A. Yu., and
816 Seppälä, A.: Mesosphere-to-stratosphere descent of odd nitrogen in February–March 2009
817 after sudden stratospheric warming, *Atmos. Chem. Phys.*, 11, 4645–4655,
818 <https://doi.org/10.5194/acp-11-4645-2011>, 2011.

819 Scheiben, D., Straub, C., Hocke, K., Forkman, P., and Kämpfer, N.: Observations of middle
820 atmospheric H₂O and O₃ during the 2010 major sudden stratospheric warming by a network
821 of microwave radiometers, *Atmos. Chem. Phys.*, 12, 7753–7765,
822 <https://doi.org/10.5194/acp-12-7753-2012>, 2012.

823 Shepherd, M. G., Beagley, S. R., and Fomichev, V. I.: Stratospheric warming influence on the
824 mesosphere/lower thermosphere as seen by the extended CMAM, *Ann. Geophys.*, 32, 589–
825 608, doi:10.5194/angeo-32-589-2014, 2014.

826 Solomon, S., Garcia, R. R., Olivero, J. J., Bevilacqua, R. M., Schwartz, P. R., Clancy, R. T., and
827 Muhleman, D. O.: Photochemistry and transport of carbon monoxide in the middle
828 atmosphere, *J. Atmos. Sci.*, 42, 1072–1083, 1985.

829 Stray, N. H., Orsolini, Y. J., Espy, P. J., Limpasuvan, V., and Hibbins, R. E.: Observations of
830 planetary waves in the mesosphere-lower thermosphere during stratospheric warming
831 events, *Atmos. Chem. Phys.*, 15, 4997–5005, <https://doi.org/10.5194/acp-15-4997-2015>,
832 2015.

833 Tao, M., Konopka, P., Ploeger, F., Grooß, J.-U., Müller, R., Volk, C. M., Walker, K. A., and
834 Riese, M.: Impact of the 2009 major sudden stratospheric warming on the composition of
835 the stratosphere, *Atmos. Chem. Phys.*, 15, 8695–8715, <https://doi.org/10.5194/acp-15-8695-2015>, 2015.

837 Taguchi, M.: Comparison of subseasonal-to-seasonal model forecasts for major stratospheric
838 sudden warmings, *J. Geophys. Res.-Atmos.*, 123, 10,231–10,247,
839 doi:10.1029/2018jd028755, 2018.

840 Tomikawa, Y., Sato, K., Watanabe, S., Kawatani, Y., Miyazaki, K., and Takahashi, M.: Growth
841 of planetary waves and the formation of an elevated stratopause after a major stratospheric
842 sudden warming in a T213L256 GCM, *J. Geophys. Res.*, 117, D16101,
843 doi:10.1029/2011JD017243, 2012.

844 Tripathi, O. P., Baldwin, M., Charlton-Perez, A., Charron, M., Cheung, J. C. H., Eckermann, S.
845 D., Gerber, E., Jackson, D. R., Kuroda, Yu., Lang, A., McLay, J., Mizuta, R., Reynolds, C.,
846 Roff, G., Sigmond, M., Son, S.-W., and Stockdale, T.: Examining the predictability of the
847 stratospheric sudden warming of January 2013 using multiple NWP systems, *Mon. Weather
848 Rev.*, 144, 1935–1960, doi:10.1175/mwr-d-15-0010.1, 2016.

849 Vargin, P. N. and Kiryushov, B. M.: Major sudden stratospheric warming in the Arctic in
850 February 2018 and its impacts on the troposphere, mesosphere, and ozone layer, *Russian
851 Meteorology and Hydrology*, 44, 112–123, doi:10.3103/S1068373919020043, 2019.

852 Waters, J. W., Wilson, W. J., and Shimabukuro, F. I.: Microwave measurement of mesospheric
853 carbon monoxide, *Science*, 191, 1174–1175, doi:10.1126/science.191.4232.1174, 1976.

854 WMO Commission for Atmospheric Sciences. Abridged Final Report of the Seventh Session,
855 Manila, 27 February – 10 March, 1978. WMO-No. 509, 113 p., available at:
856 http://library.wmo.int/pmb_ged/wmo_509_en.pdf, 1978.

857 Xu, X., Manson, A. H., Meek, C. E., Chshyolkova, T., Drummond, J. R., Hall, C. M., Riggan,
858 D. M., and Hibbins, R. E.: Vertical and interhemispheric links in the stratosphere-
859 mesosphere as revealed by the day-to-day variability of Aura-MLS temperature data, *Ann.
860 Geophys.*, 27, 3387–3409, doi:10.5194/angeo-27-3387-2009, 2009.

861 Yu, Y., Cai, M., Shi, C., and Ren, R.: On the linkage among strong stratospheric mass
862 circulation, stratospheric sudden warming, and cold weather events, *Mon. Weather Rev.*,
863 146, 2717–2739, doi:10.1175/MWR-D-18-0110.1, 2018.

864 Yuan, T., Thurairajah, B., She, C. Y., Chandran, A., Collins, R. L., and Krueger, D. A.: Wind
865 and temperature response of midlatitude mesopause region to the 2009 Sudden
866 Stratospheric Warming, *J. Geophys. Res.*, 117, D09114, doi:10.1029/2011JD017142, 2012.

867 Zhou, S., Miller, A. J., Wang, J., and James, K. A.: Downward-propagating temperature
868 anomalies in the preconditioned polar stratosphere, *J. Climate*, 15, 781–792,
869 doi:10.1175/1520-0442(2002)015<0781:DPTAIT>2.0.CO;2, 2002.

870 Zülicke, C. and Becker, E.: The structure of the mesosphere during sudden stratospheric
871 warmings in a global circulation model, *J. Geophys. Res.-Atmos.*, 118, 2255–2271,
872 doi:10.1002/jgrd.50219, 2013.

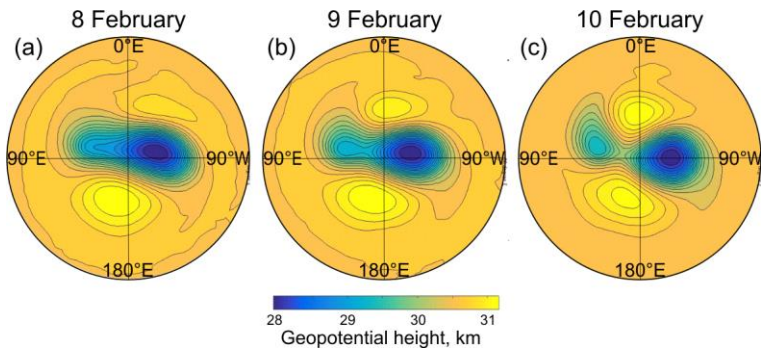
873 Zülicke, C., Becker, E., Matthias, V., Peters, D. H. W., Schmidt, H., Liu, H.-L., de la Torre
874 Ramos, L., and Mitchell, D. M.: Coupling of stratospheric warmings with mesospheric
875 coolings in observations and simulations, *J. Climate*, 31, 1107–1133, doi:10.1175/JCLI-D-
876 17-0047, 1, 2018.

877

878

879

880

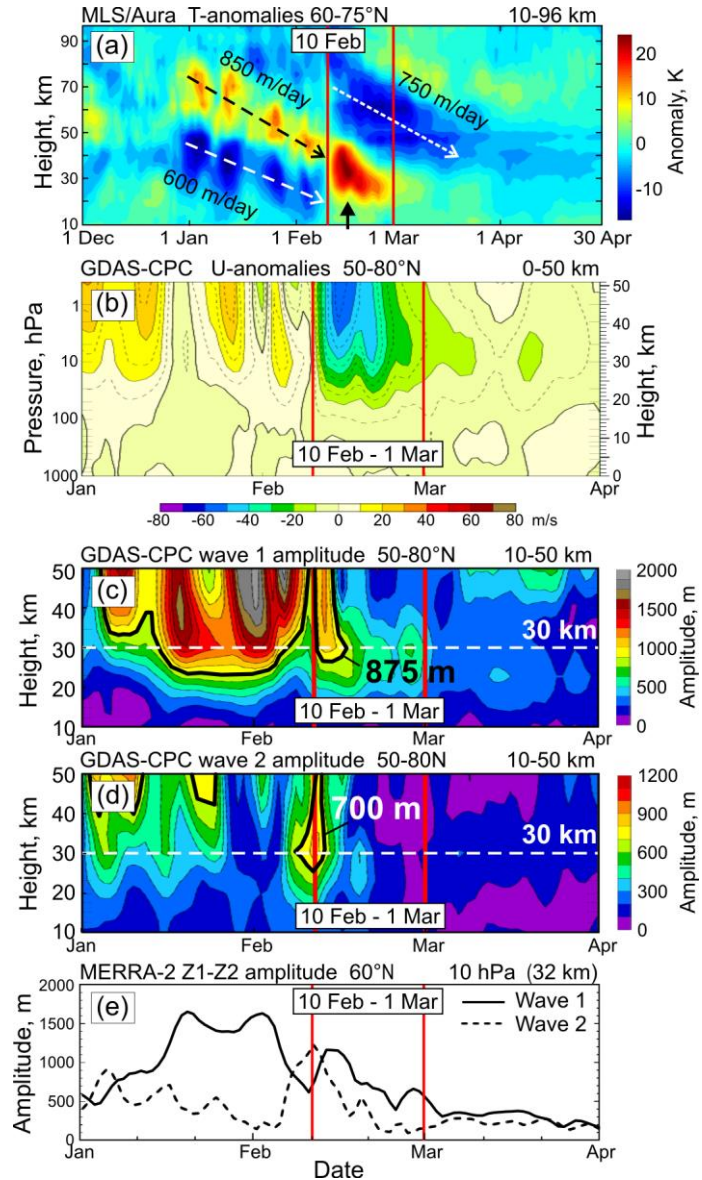


881

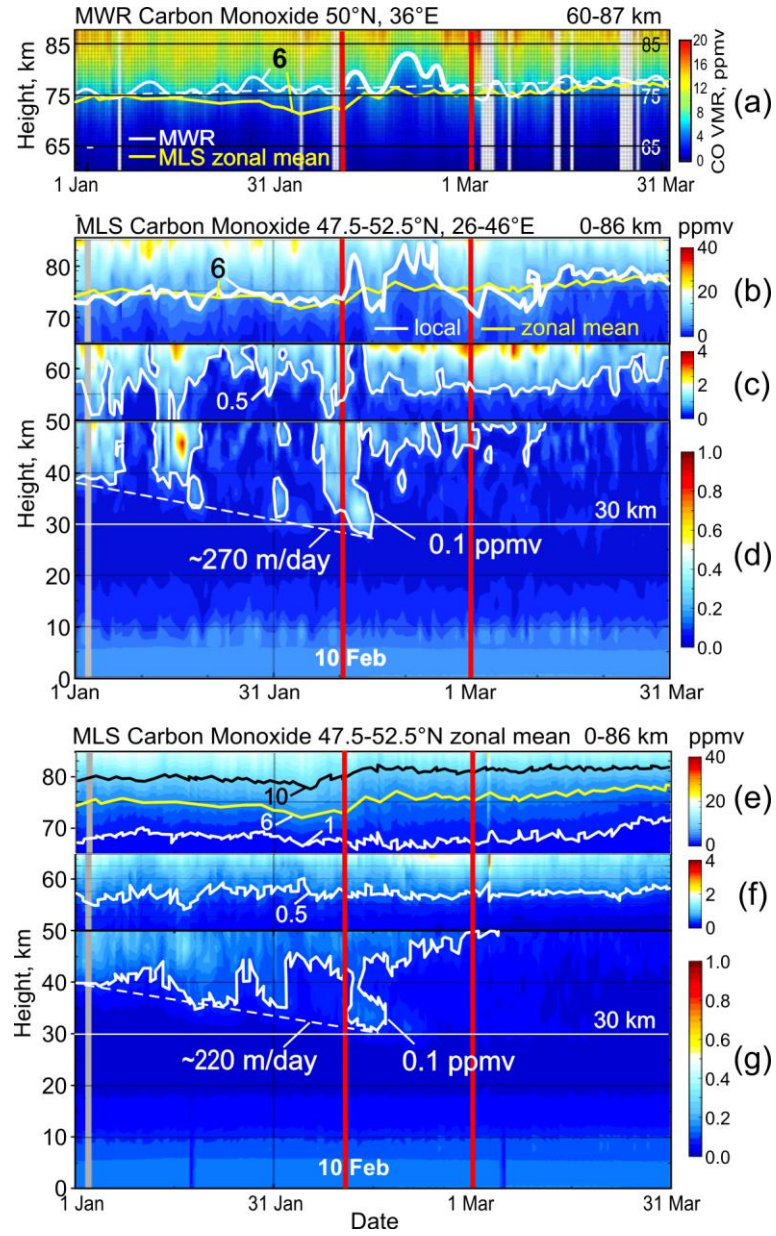
882

883 **Figure 1.** The polar vortex split at the 10-hPa pressure level during the SSW event in February
884 2018. Geopotential heights are calculated from ERA-Interim reanalysis data.

885

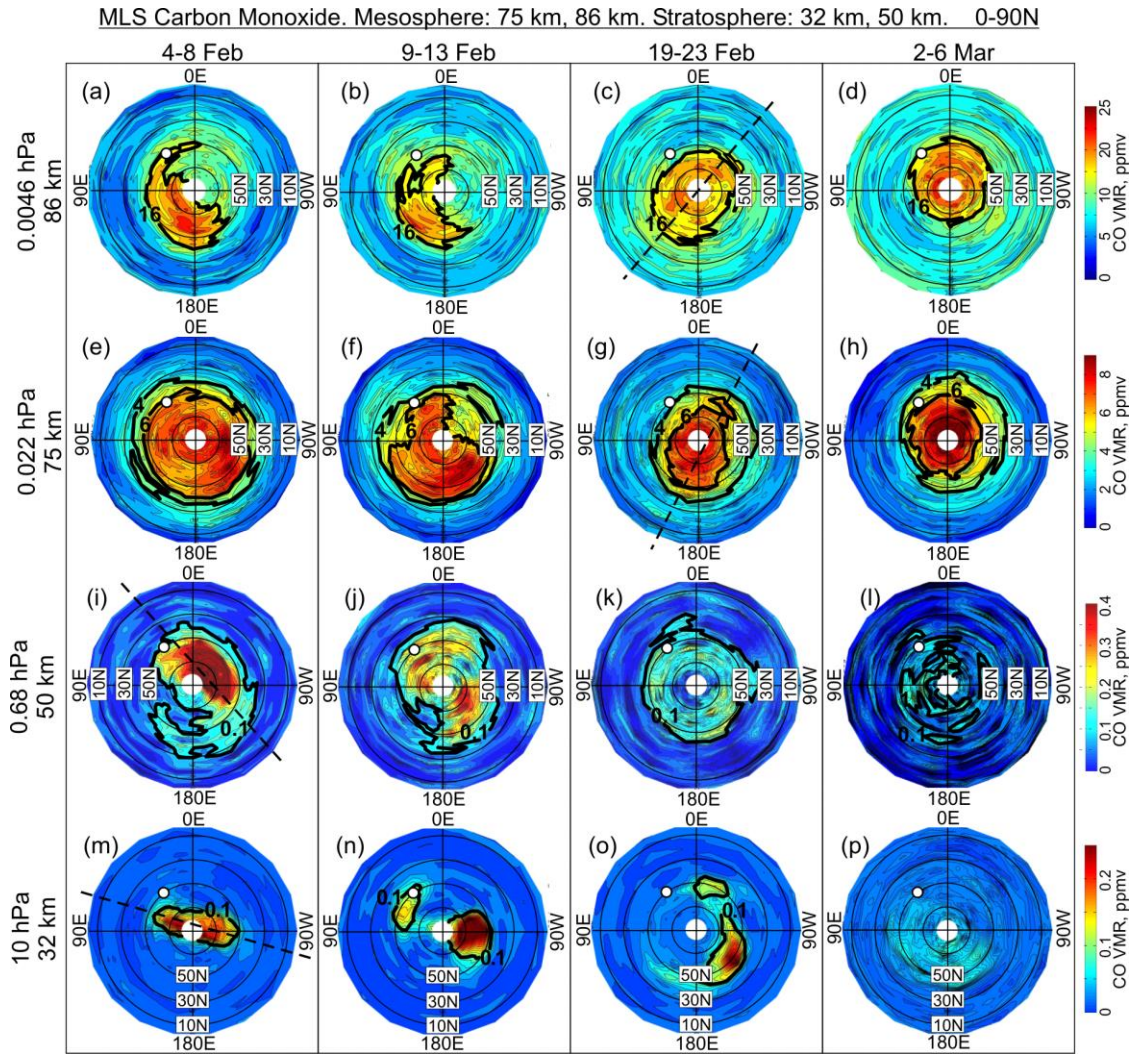


889 **Figure 2.** The development of the SSW in 2018 from the vertical profiles of (a) Aura MLS
 890 temperature anomalies in December 2017–April 2018 at polar zone 60–75°N (with respect to
 891 the mean climatology 2005–2017), (b) zonal mean zonal wind anomalies, (c) wave 1 and (d)
 892 wave 2 amplitudes in geopotential height in January–March by NOAA NCEP GDAS-CPC data
 893 (climatology 1981–2010). (e) zonal wave 1 and wave 2 amplitudes in geopotential height at 10
 894 hPa, 60°N, by the MERRA-2 time series from the NASA GFC ACDL data. The SSW-related
 895 anomalous variability between 10 February and 1 March 2018 is bounded by red vertical lines.
 896



901 **Figure 3.** (a) Mesospheric CO profile from microwave measurements over Kharkiv averaged
 902 in altitude range 70–85 km, and vertical CO profile from the MLS measurements averaged over
 903 latitudes 47.5–52.5°N and longitudes (b)–(d) 26–46°E centered at the Kharkiv MWR site
 904 (50°N, 36°E) and (e)–(g) 0–360°E for zonal mean. Selected CO levels are highlighted by white,
 905 black and yellow contours (see text for details). Data for January–March 2018 are presented
 906 and time interval of significant variations in the atmosphere parameters due to the SSW event
 907 (from 10 February to 1 March 2018) is bounded by red vertical lines.

910
911
912



913
914

915 **Figure 4.** The 5-day mean CO field over the NH (0–90°N) from the MLS measurements at the
916 two mesospheric (75 km and 86 km) and stratospheric (32 km and 50 km) levels before (4–8
917 February), during (9–13 and 19–23 February) and after (2–6 March) the SSW 2018. White
918 circle shows location of the MWR site Kharkiv relatively the high/low CO amounts marked off
919 by the black contours. Dashed lines indicate clockwise rotation of the elongated polar vortex
920 with altitude as manifestation of upward propagation of planetary waves with their westward
921 tilt with altitude.

922
923
924

925

926

927

928

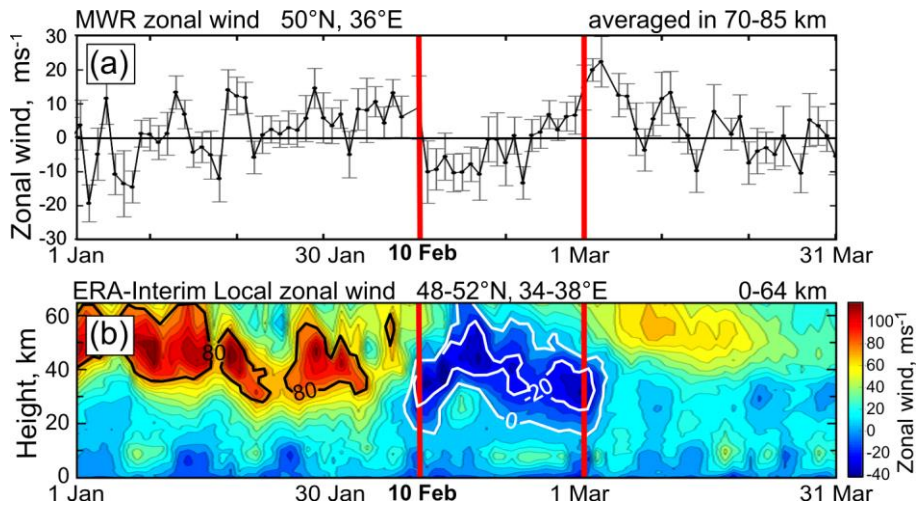
929

930 **Figure 5.** (a) Mesospheric zonal wind microwave measurements over Kharkiv (averaged in
 931 altitude range 70–85 km, vertical bars are standard deviations) compared to (b) time-altitude
 932 local zonal wind from the ERA-Interim reanalysis data averaged over latitudes 48–52°N and
 933 longitudes 34–38°E (centered at the Kharkiv microwave radiometer site, 50°N, 36°E). Time
 934 interval of significant variations in the atmosphere parameters due to the SSW event (from 10
 935 February to 1 March, 2018) is bounded by red vertical lines.

936

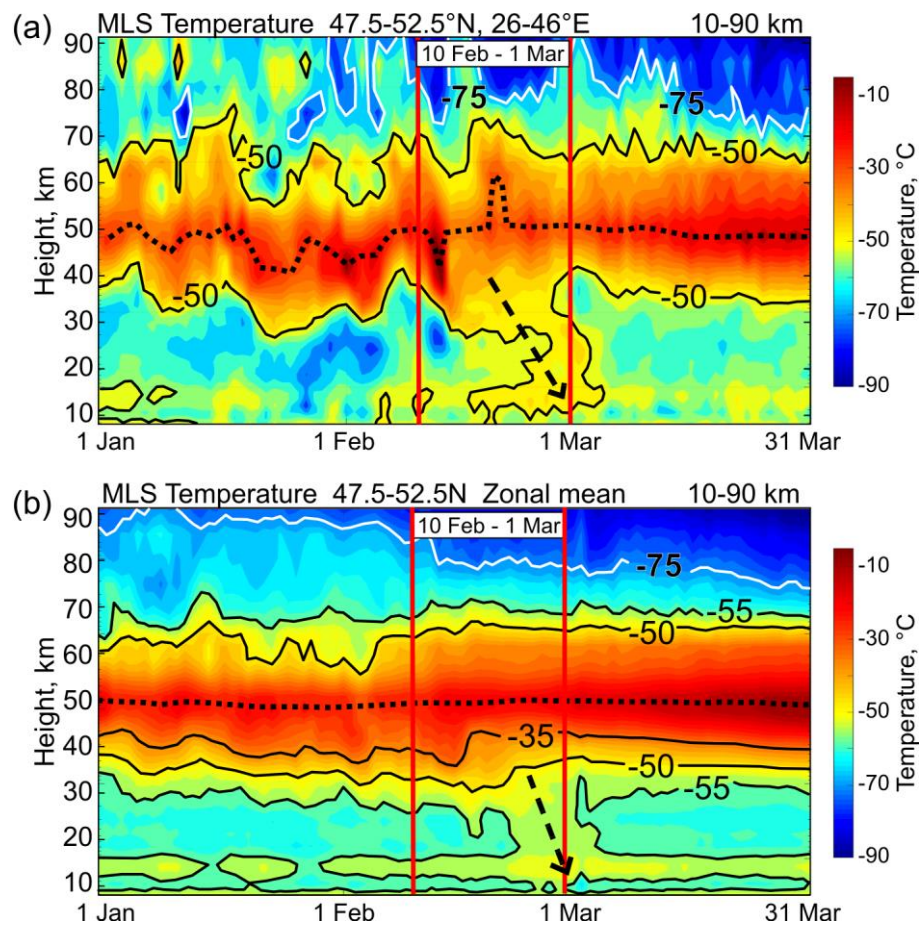
937

938



939

940



941

942

943 **Figure 6.** MLS temperature profiles (a) over the Kharkiv region and (b) zonal average in the
 944 zone 47.5–52.5°N. Dashed arrows indicate downward warming.

945

946

947

Supplementary Material

Winter 2018 major sudden stratospheric warming impact on midlatitude mesosphere from microwave radiometer measurements, by Wang et al.

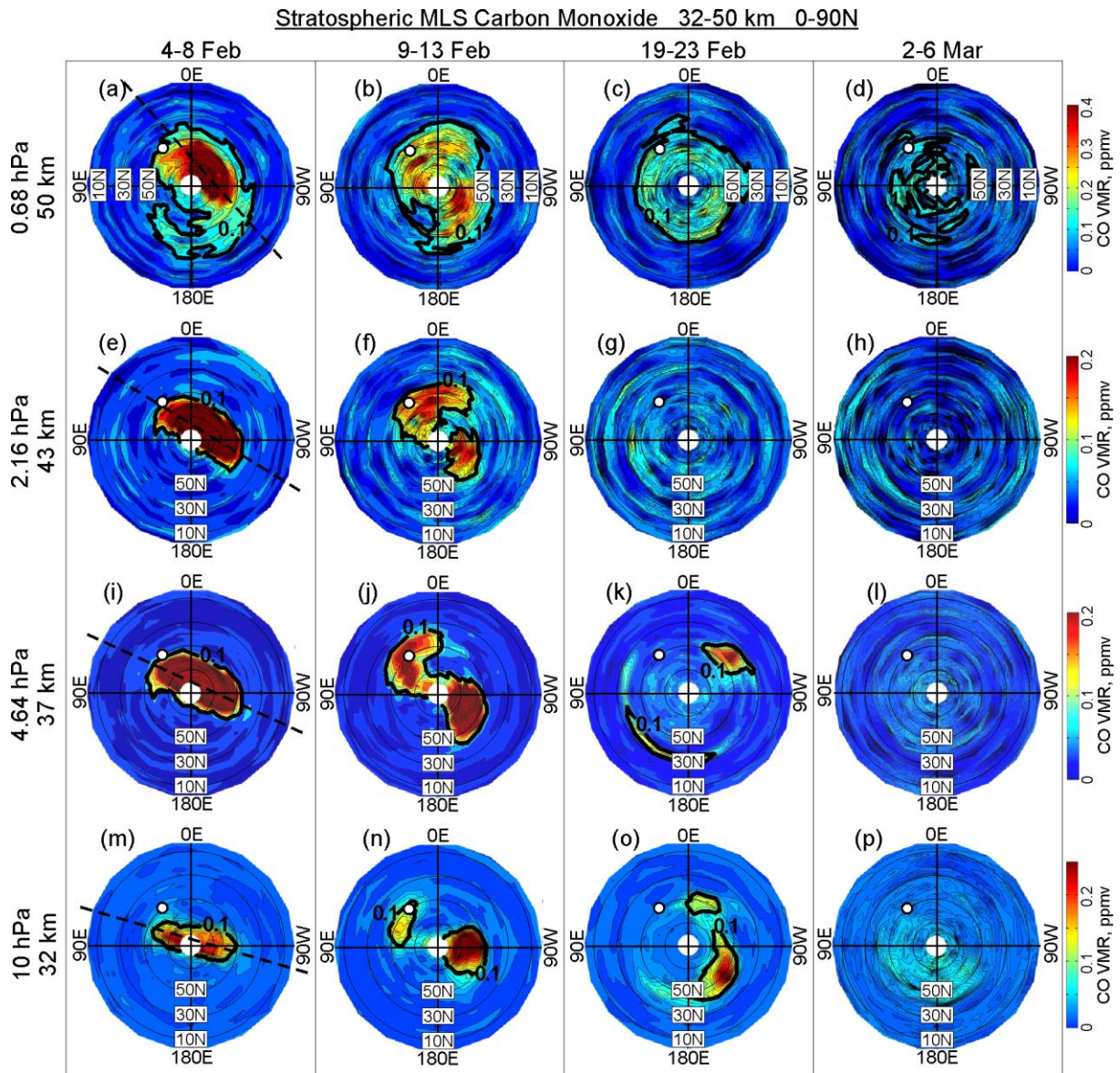
The description of the data used for analysis

7 The Aura MLS CO values have been taken from version 4.2x Aura MLS Level 2 data
8 (<https://mls.jpl.nasa.gov/data/readers.php>). Aura MLS v4.2x data have 37 pressure levels. The
9 useful range of CO data is from 215 hPa to 0.0046 hPa with corresponding height is from ~11
10 km to ~86 km. The satellite observation data points are divided into 20° longitude \times 2° latitude
11 grids. That means: longitude is divided into $180^\circ:20^\circ:180^\circ$ and latitude is divided into
12 $90^\circ:2^\circ:90^\circ$ segments. Then the average value of the data is taken in the grid as the value of the
13 center of the grid. For instance, the average in the grid of 180° – 160° in longitude and 90° – 88°
14 in latitude is taken as the average value of 170° degrees in longitude and 89° in latitude.

15 Data are removed (replaced by ‘NaN’) if they do not meet the quality criteria described in
16 ‘Version 4.2x Level 2 data quality and description document’ (https://mls.jpl.nasa.gov/data/v4-2_data_quality_document.pdf). The five-day average (Fig. S1 and S2) is not simply a sum,
17 divided by five. If the data of a certain area is blank, the data of that area will be ignored on that
18 day. For example, if the data of a certain area in five days are: A, B, NaN, C, NaN, the average
19 value of this area is $(A+B+C)/3$.
20

Daily datasets from ERA-Interim global atmospheric reanalysis of European Centre for Medium-Range Weather Forecast have been used for comparison with microwave radiometer observations (<https://www.ecmwf.int/en/forecasts/datasets/archive-datasets/reanalysis-datasets/era-interim>). Two types of level in the ERA-Interim database were used: ‘Model level’ and ‘Pressure level’. The number vertical levels in ‘Model level’ and ‘Pressure level’ datasets are 60 and 37, respectively. The pressure ranges in ‘Model level’ and ‘Pressure level’ datasets are from the surface up to 0.1 hPa and 1 hPa, respectively. Horizontal dimension resolution (longitude×latitude) is selected as $0.75^\circ \times 0.75^\circ$. The ‘Model type’ data are used for drawing temperature and zonal wind velocity profiles from surface up to 0.1 hPa in order to compare with the data measured by microwave radiometer in Kharkiv, which extends up to 87 km altitude. The ‘Pressure level’ data were used to create geopotential height plots (Fig. 1).

CO movements in stratosphere and mesosphere



35 **Figure S1.** The 5-day mean CO field in the NH stratosphere (0–90°N, between 32 km and 50
 36 km) from the MLS measurements before (first column, 4–8 February), during (second and third
 37 columns, 9–13 and 19–23 February, respectively) and after (forth column, 2–6 March) the SSW
 38 2018. White circle shows location of the MWR site Kharkiv relatively the high/low CO
 39 amounts marked off by the black contours. Note that Kharkiv falls under the area of high CO
 40 amount just after the SSW start (second column, 9–13 February) due to the westward rotation
 41 of the polar air mass caused by the zonal wind reverse from westerly to easterly. The high CO
 42 anomalies disappear after the SSW (right column, 2–6 March). Dashed lines indicate planetary
 43 wave westward tilt with altitude.

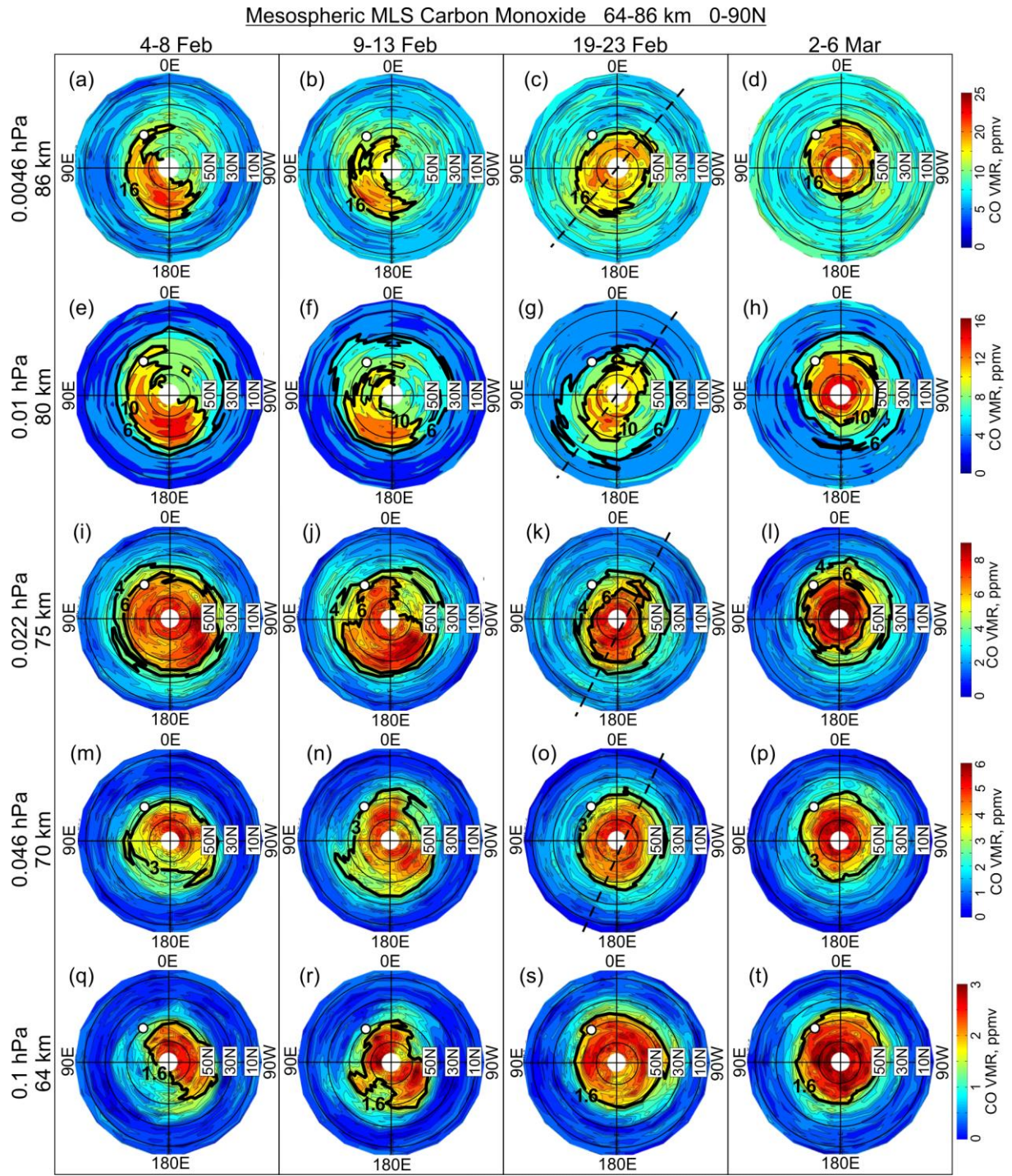
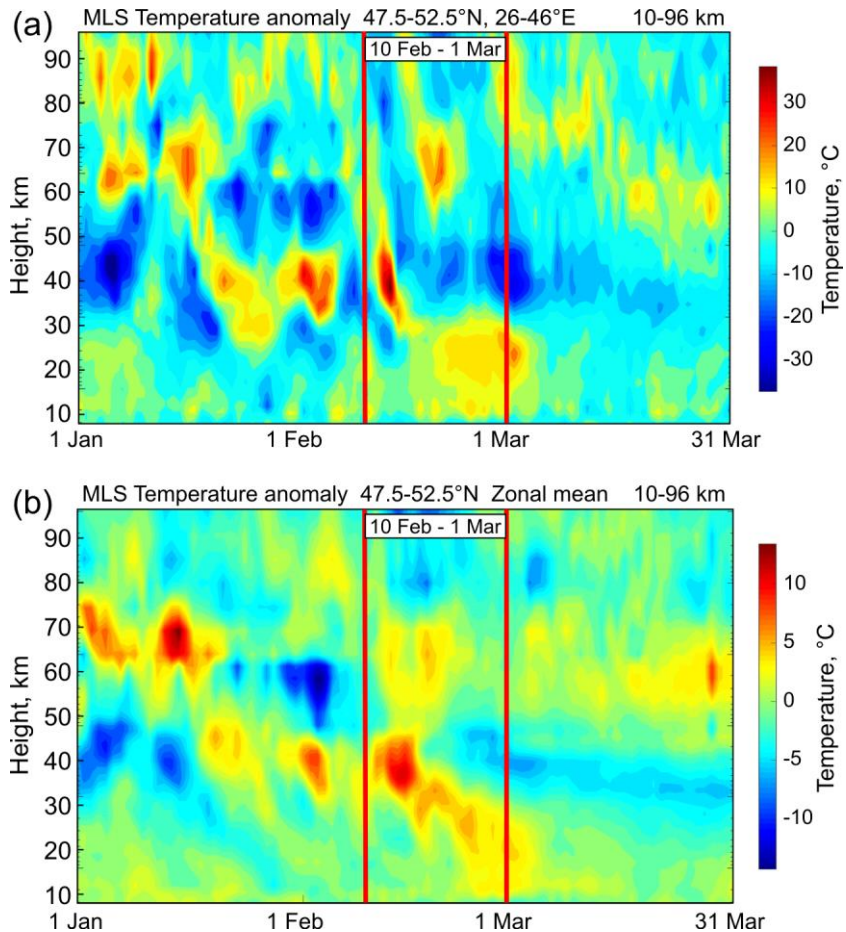


Figure S2. As in Fig. S1, but for the NH mesosphere (0–90°N, between 64 km and 86 km). Note that the lowest mesospheric CO levels observed with the MWR in February 2018 over Kharkiv (white curve for 6 ppmv in Fig. 3a) are explained by the westward displacement of the boundary between the low- and high-CO polar air mass (compare the Kharkiv location relative to the contour 16 ppmv in (a–c), 6 ppmv in (e–g) and 4 ppmv in (i–k) at 86, 80 and 75 km, respectively. Dashed lines indicate planetary wave westward tilt with altitude.

53

54



55

56

57

58

59

Figure S3. Vertical profiles of the MLS temperature anomalies in January–March 2018 with respect to the mean climatology 2005–2017 over (a) region 47.5–52.5°N, 26–46°E centered at Kharkiv and (b) 47.5–52.5°N zonal mean centered at the Kharkiv latitude. Red vertical lines confine the SSW event 2018.

60

61

62